Glacial-interglacial variations of the water masses in the southeast Atlantic Ocean derived from foraminiferal neodymium isotope ratios

Rebecca von Koslowski

A minor dissertation submitted in partial fulfillment
of the requirement for the degree of

Master of Science (M.Sc.)
in Applied Marine Sciences

in the department of
Biological Sciences
and the
Marine Research Institute

University of Cape Town

March 2017

Supervisor: Assoc. Prof. John Compton
Department of Geological Sciences

[This page intentionally left blank]

PLAGIARISM DECLARATION

I know the meaning of plagiarism and that plagiarism is wrong. With my signature, I certify that this dissertation has been written by me using only the indicated resources and materials, which have been cited and referenced using the standard reference style of the journal *Paleoceanography*. Where I have presented data and results, the data and results are complete, genuine, and have been obtained by me unless otherwise acknowledged; where my results derive from computer programs, these computer programs have been written by me unless otherwise acknowledged. I further confirm that this thesis has not been submitted, either in part or as a whole, for any other academic degree at this or another institution. I have not allowed, nor will I allow, anyone to copy my work with the intention of passing it of as their own work. I acknowledge that copying someone else's assignment or essay, or part of it, is wrong and I declare that this is my own work.

Cape Town, South Africa, the 13th of March 2017

Signed by candidate

Rebecca von Koslowski

[This page intentionally left blank]

ABSTRACT

Variations in the global climate over time have long been associated with changes in the meridional overturning circulation of the oceans. It is now commonly believed that, during the Last Glacial Maximum (LGM), the transport of North Atlantic Deep Water (NADW) to the southeast Atlantic Ocean was reduced. A popular method to trace these ambient changes is the stable isotope systematics of neodymium (given as ε_{Nd}). In this study ε_{Nd} data were measured on mixed planktic and bulk foraminifera from two gravity cores, GeoB8336-6 and GeoB8342-6, retrieved from the Cape Basin at water depths of 3524 and 3521 meters from the western continental slope of South Africa.

The samples were prepared following the protocol presented by the Cambridge group [*Tachikawa et al.*, 2014]. Planktic and bulk foraminifera samples taken from the same core depth interval had the same ε_{Nd} ratios within error, which suggests that bulk foraminifera may provide a quick way to reconstruct ambient bottom water values. However, more research is needed to further support these findings. While the Holocene samples' ε_{Nd} ratios ($\varepsilon_{Nd(N36/6a)}$ -10.7±0.3 and $\varepsilon_{Nd(N42/6a\ mean)}$ -10.2±0.4) lie within the range of modern Eastern NADW ($\varepsilon_{Nd(modern\ ENADW)}$ -10.9±1.2), glacial samples yield significantly more radiogenic ε_{Nd} ratios ($\varepsilon_{Nd(N42/6b)}$ -7.7/ $\varepsilon_{Nd(N36/6b)}$ -8.1). This indicates the greater influence of southern-sourced water masses and thus provides further evidence for a reduction of NADW during the last glacial. MIS3 samples show ratios that lie in between those observed in the LGM and Holocene, and it is hypothesized that ocean circulation during MIS3 was comparable to that during the transition from the LGM to the Holocene (Termination I).

[This page intentionally left blank]

TABLE OF CONTENTS

[This page intentionally left blank]

[This page intentionally left blank]

1 INTRODUCTION

1.1 THE ATLANTIC MERIDIONAL OVERTURNING CIRCULATION

The global oceans are connected through the Meridional Overturning Circulation (MOC), a complex network of surface currents and deep water flows, mostly driven by wind and tidal energy, freshwater fluxes, and differences in temperature and buoyancy. The MOC exports surface water into the deep sea and brings deep ocean water to the ocean-atmosphere interface, and thus plays a crucial role in the oceans' salt, carbon, nutrient and heat exchange [*Lumpkin and Speer*, 2007; *Schmittner et al.*, 2007]. The Atlantic component of the MOC, the Atlantic Meridional Overturning Current (AMOC), is one of the major drivers of this 'conveyor belt', and therefore of particular importance to the global heat exchange. The modern AMOC is characterized by northward flowing warm surface and intermediate waters (<1000 m) (Antarctic Intermediate Water; AAIW), which continuously decrease in buoyancy until they finally become dense enough to sink down in the Nordic seas near Iceland, Greenland, Norway and Scotland. This descending water becomes the southward flowing North Atlantic deep water (NADW), a cold and salty water mass that exports carbon and nutrient-rich water from the North Atlantic into the deep South Atlantic [*Sverdrup et al.*, 1942; *Emery, W. J., Meincke*, 1986; *Duplessy et al.*, 1988; *Broecker and Denton*, 1990; *Clark et al.*, 2002; *Lynch-Stieglitz et al.*, 2007; *Delworth et al.*, 2008]. NADW forms in the North Atlantic mostly as a result of cooling in the higher latitudes, however, it is now commonly believed that the preconditioning essential to the amplitude of the formation already starts in the southeast Atlantic, just off the coast of Southern Africa [*Lutjeharms and van Ballegooyen*, 1988; *Broecker and Denton*, 1990; *Gordon et al.*, 1992; *de Ruijter et al.*, 1999; *Delworth et al.*, 2008]. Here, the Agulhas Current carries warm water from the Indian

Ocean along the east coast of southern Africa to the Agulhas Bank where it retroflects and flows back eastwards [*Lutjeharms and van Ballegooyen*, 1988; *Peterson and Stramma*, 1991; *Stramma and England*, 1999; *Lutjeharms and Ansorge*, 2001]. However, not all water is returned into the Indian Ocean: some of the subtropical water flows into the cold southeast Atlantic (Agulhas leakage) either directly as filaments or as mesoscale eddies – Agulhas 'rings' [*Lutjeharms et al.*, 1991; *Beal et al.*, 2011]. The temperature differences between the Atlantic and Indian waters induce evaporation, leaving the northward flowing water more saline and dense [*Lutjeharms and van Ballegooyen*, 1988; *Duncombe Rae*, 1991; *Gordon et al.*, 1992; *de Ruijter et al.*, 1999]. Additionally, the movement of NADW is affected by the travel path of the Agulhas rings: as the warm, salty water inclusions advance into the southeastern Atlantic, they create an eddy thickness flux, which shifts the movement of NADW [*Weijer et al.*, 2001, 2002; *Beal et al.*, 2011; *van Sebille et al.*, 2012]. This forces the deep water mass to circulate through the Basin. The direct interaction of lower and upper circulation of the meridional overturning current in the Cape Basin, suggests that the strength of the MOC is directly affect by the extent of the Agulhas leakage [*van Sebille et al.*, 2012].

In addition to the upper circulation cell, Antarctic Bottom Water (AABW), a very cold, dense water mass that forms down near Antarctica, travels northward below 4000 m and enters the South Atlantic below the NADW [e.g. *Schmittner et al.*, 2013]. In comparison to the upper circulation, which exhibits temperature differences of up to ~15°C between the surface and lower water masses, the circulation of AABW is of far lesser importance for the global heat transport [*Delworth et al.*, 2008].

CLIMATE CHANGE-INDUCED VARIABILITY OF THE MOC

As first noted by Mulitin Milankovitch, the Earth undergoes periodic episodes of warming and cooling (glacial-interglacial cycles), which can be attributed to variations in its orbital shape (eccentricity), axial tilt (obliquity) and axial precession. These three phenomena are collectively referred to as 'Milankovitch cycles', and occur in periods of ~100,000, 41,000, and 23,000 years, respectively [*Berger et al.*, 1984; *Imbrie et al.*, 1992].

Since the formation of deep water is largely driven by temperature and density differences, the MOC is very sensitive to variations in the global climate [*Schmittner et al.*, 2007]. Abrupt changes in the

global climate in the past have been linked to shifts in ocean circulation and the export of water masses in the Atlantic Ocean (Figure 1) [*Clark et al.*, 2002; *Lynch-Stieglitz et al.*, 2007]. During the last glacial maximum (LGM) (centered around 23 ka), for instance, changes in the Earth's climate, the global ice masses and carbon budget led to variations in the MOC [*Curry and Oppo*, 2005; *Piotrowski et al.*, 2005; *Lynch-Stieglitz et al.*, 2007; *Marchal and Curry*, 2008]. It is now commonly believed that the Agulhas leakage was weakened [*Franzese et al.*, 2006] and the export of warm water into the South Atlantic was lessened during the colder periods [*Boyle and Keigwin*, 1982; *Curry and Lohmann*, 1982; *Oppo and Fairbanks*, 1987; *Duplessy et al.*, 1988; *Rutberg et al.*, 2000; *Howe et al.*, 2016c]. This allowed for glacial AABW (GAABW) to enter further into the South Atlantic [*Oppo and Fairbanks*, 1987; *Duplessy et al.*, 1988; *Rutberg et al.*, 2000; *Howe et al.*, 2016a]. (Glacial) AAIW is believed to have remained unchanged since the LGM [*Howe et al.*, 2016a].

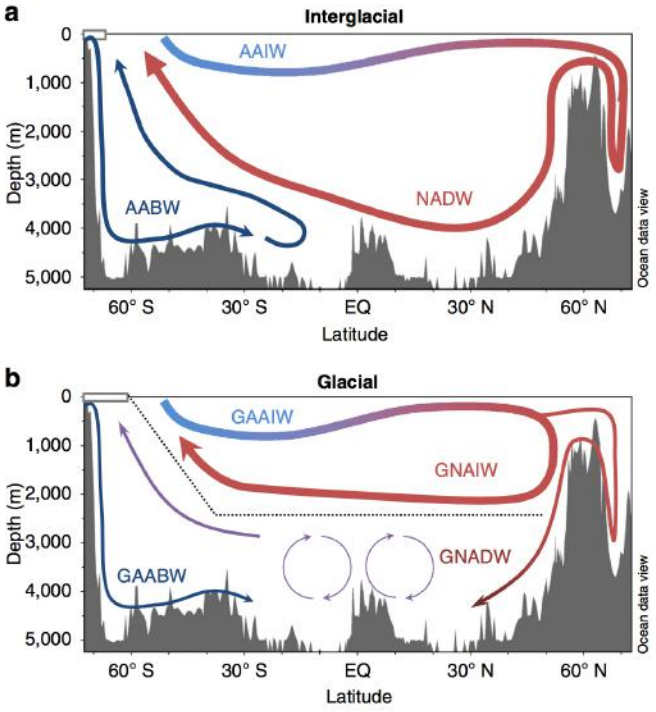

Figure 1. Proposed circulation scheme for the interglacial (a) and glacial (b) Atlantic. Warm water masses are indicated in red, cold water masses are shown in blue. The water masses of the interglacial are Antarctic Intermediate Water (AAIW), North Atlantic Deep Water (NADW), and Antarctic Bottom Water (AABW); those of the glacial are Glacial AAIW (GAAIW), Glacial North Atlantic Intermediate Water (GNAIW), Glacial NADW (GNADW), and Glacial AABW (GAABW).

The ocean circulation mechanisms are described in the text [graphic taken from *Howe et al.*, 2016c].

The water masses did not only vary in their lateral extent: water mass reconstruction records of glacial NADW (GNADW) from the last glacial indicate significant shoaling of up to 1000 m in comparison to the modern NADW [e.g. *Curry and Lohmann*, 1982; *Duplessy et al.*, 1988; *Gebbie*, 2014]. These distinct differences first led to the establishment of a new water mass, glacial North Atlantic Intermediate Water, which was initially believed to have replaced NADW during the glacial entirely [*Boyle and Keigwin*, 1987; *Duplessy et al.*, 1988]. However, recent studies suggest a subdivide of the

glacial Atlantic waters into two water masses, the denser waters below 2500 m are believed to form GNADW, while those waters shallower than 2500 m are now considered to be Glacial North Atlantic Intermediate Water (GNAIW) [*Howe et al.*, 2016c and references therein].

As pointed out before, the MOC is of great significance for the global heat exchange, and, while the circulation variations during the LGM were not the initial reason for the rapid cooling, they are believed to have at least amplified the cooling process significantly on a millennial scale [*Broecker*, 1982; *Broecker and Denton*, 1990; *Rutberg et al.*, 2000; *Kerr*, 2005]. Hence, to study the climate of the past, it is of great importance to have a good understanding of the variations in the ambient water masses. Tracing (ancient) water masses and studying the variations of their extent between the interglacial and glacial periods can provide a powerful tool for a better understanding of climate change, and helps shed light on the importance of (global) scale climate variations on the thermohaline circulation, and vice versa [e.g. *Clark et al.*, 2002; *Piotrowski et al.*, 2005].

1.2 TRACING (ANCIENT) WATER MASSES

Water masses are water bodies with a common formation history that originate from the same source region in which they acquire specific physical and chemical water properties [*Emery, W. J., Meincke*, 1986, and references therein]. While salinity and temperature are well-known properties used to quickly identify modern water masses [*Emery, W. J., Meincke*, 1986], distinguishing between ancient water masses requires a different approach as these properties are not directly conserved over time. Hence, to trace ancient water masses, it is important to find an appropriate tracer that reliably shows the distinct differences of various water masses and thus allows for the identification of water masses, and to identify a suitable substrate that acts as a seawater archive and conserves these tracer signatures. If unaltered by secondary, syn- or post-depositional processes, marine sediments preserve the geochemical signature of the ambient seawater they form from and are exposed to. Thus, they can provide a powerful tool for many (paleo-)environmental and –oceanographic applications [e.g. *Vance et al.*, 2004; *Claude and Hamelin*, 2007; *Li and Schoonmaker*, 2013]. The study of the geochemical composition of marine sediments such as manganese nodules [*Piepgras et al.*, 1979; *von*

Blankenburg, 1999; *Li and Schoonmaker*, 2013], authigenic[1] Fe-Mn crusts [*Gutjahr et al.*, 2007] and sedimentary foraminifera [*Rutberg et al.*, 2000; *Tachikawa et al.*, 2014], for instance, proved to be a good tool to reconstruct the ambient ocean circulation.

Stable isotope ratios of carbon ($\delta^{13}C$), often combined with Cd/Ca ratios, is the most commonly used tracer for water masses [*Lynch-Stieglitz and Marchitto*, 2013]. $\delta^{13}C$ ratios are nutrient tracers, which vary depending the amount of carbon that is regenerated as the water masses get older, and thus are a good indicator for water masses. However, when preserved in marine organisms, such as foraminifera, the radiocarbon systematics are not always representative of the water they formed from: they can be affected by various physical and biochemical factors and processes, for instance ambient seawater temperature, the nutrient and carbonate availability [*von Blankenburg*, 1999 and references therein; *Lynch-Stieglitz and Marchitto*, 2013]. A frequently used application that addresses this issue and has proven to defy fractionation by productivity changes [*Rutberg et al.*, 2000] is the isotope composition of the rare earth element (REE) neodymium. Different $^{143}Nd/^{144}Nd$ ratios in Earth are a result of the α-decay of ^{147}Sm, with a half-life of ~106 $*10^9$ years [*Goldstein and Hemming*, 2013], and are commonly given as

$$\varepsilon_{Nd} = \left[\frac{(^{143}Nd/^{144}Nd)_{sample}}{(^{143}Nd/^{144}Nd)_{CHUR}} - 1\right] * 10^4,$$

where ε_{Nd} denotes the deviation of measured $^{143}Nd/^{144}Nd$ of a sample from the present day bulk earth value of the $^{143}Nd/^{144}Nd$ ratio measured in chondrites and expressed as "CHUR" (chondritic uniform reservoir) (present value: $^{143}Nd/^{144}Nd$ = 0.512638) in parts per ten thousand [*Jacobsen and Wasserburg*, 1980]. Nd is estimated to have a residence time of 200 to 1000 years [*Jeandel*, 1993; *Tachikawa et al.*, 1999], which is less than the ocean's turnover rate [*Wei et al.*, 2016]. It enters the oceans through the weathering of continental clay-rich sediments [*Piepgras and Wasserburg*, 1980], so that the $^{143}Nd/^{144}Nd$ in seawater reflect the age of dissolved terrigenous Nd [*Piotrowski et al.*, 2005]. Therefore, the ε_{Nd} of different water masses are distinctive and represent their formation origin.

[1] Authigenic sediments that formed in the same region they are found in today, as opposed to allogenic sediments, which formed elsewhere and were then transported [*Neuendorf*, 2005]

Provided that these sediments were not substantially affected by any secondary processes [e.g. *Franzese et al.*, 2006], the distinctive differences in the Nd isotopic compositions make ε_{Nd} ratios a reliable tool for tracing (ancient) water masses.

Seawater Nd isotopic ratios vary from ε_{Nd} ~-20 in the Labrador Sea to ε_{Nd} ~0 in the northwest Pacific; NADW ε_{Nd} has an average ratio of ε_{Nd} ~-13.5, while AABW shows more radiogenic ratios of ε_{Nd} ~-8.6 to ~-9.6 [e.g. *Piepgras and Wasserburg*, 1980; *Jeandel*, 1993; *Vance and Burton*, 1999; *Stichel et al.*, 2012]. AAIW shows similar but slightly more radiogenic Nd isotope behavior than AABW (ε_{Nd} ~-8.3), which could be due to the higher influence of Pacific waters [*Jeandel*, 1993; *Stichel et al.*, 2012]. Overall, the South Atlantic has an average ratio of ε_{Nd} ~-9.2±1.5, but ratios of up to ε_{Nd} ~-6.2 have been recorded at intermediate depths in the southeast Atlantic [*Jeandel*, 1993]. These very distinct differences allow for the identification of different water masses solely based on their ε_{Nd}. Therefore, if preserved in a good substrate, ε_{Nd} associated with marine sediments, provide a good tool for the reconstruction of the pathways and composition of (ancient) water masses [*Piepgras et al.*, 1979; *Piepgras and Wasserburg*, 1980; *Grousset et al.*, 1988; *Jeandel*, 1993; *Piotrowski et al.*, 2005].

1.3 FORAMINIFERA AS ARCHIVES FOR ANCIENT SEAWATER

Foraminifera, colloquially referred to as “forams", are a group of single-celled animals commonly found in the global oceans [*Kucera*, 2007; *Kimoto*, 2015]. Depending on their habitat, foraminifera are either considered to be benthic or planktic. As the name suggests, benthic foraminifera are found in the benthic zone – on or within sediment surface of the seafloor [*Murray*, 2006]. Planktic foraminifera, on the other hand, can be found throughout the water column [*Kucera*, 2007; *Kimoto*, 2015].

Once foraminifera die, they sink to the seafloor where the tests accumulate as marine sediment [*Kucera*, 2007]. For many years now, scientists have been using these foraminifera assemblages for various (paleo-)oceanographic and environmental applications, such as the reconstruction of ambient sea surface temperatures (SST) [*Kucera*, 2007]. The small calcifying organisms further provide a good indicator for the carbon export to the seafloor [*Sarmiento et al.*, 2002], and can thus be used to

recreate the (ancient) production rates of upwelling regions [*Little et al.*, 1997; *Lynch-Stieglitz and Marchitto*, 2013]. The proxy character is not limited to purely research-based studies either: the petroleum industry uses (sedimentary) foraminifera are a bio-indicator for environmental stress assessments of marine ecosystems, such as drilling-related off-shore oil spills [*Murray*, 2006; *Denoyelle et al.*, 2010].

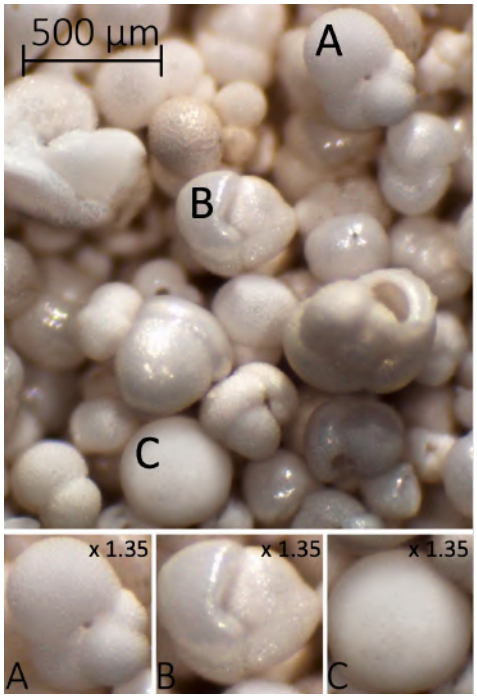

Figure 2. Mixed sedimentary foraminifera picked from sediment core GeoB8336-6 (8/9 cm), one of the cores studied in this dissertation. The magnified pictures below show *Globigerinoides sacculifer* (A), *Globorotalia inflata* (B), and the spherical *Orbulina universa* (C). The pictures of the individual tests were magnified by a factor of 1.35, i.e. the scale changes to 675 µm for these pictures.

Pictures obtained with the Leica EZ4 D microscope system at the University of Cape Town (Rebecca von Koslowski, March 2017)

Over the last few decades, foraminifera tests have become an established tool for the reconstruction of ambient water masses [e.g. *Kucera*, 2007; *Roberts et al.*, 2012; *Kraft et al.*, 2013; *Lynch-Stieglitz and Marchitto*, 2013; *Tachikawa et al.*, 2014]. An extensive assessment of rare earth elements behavior in foraminifera by Palmer [1985] concluded that foraminifera preserve REE in three different phases – in the calcite lattice tests, coatings on the tests and as detrital REE. Lattice REE are incorporated into the foraminifera calcite matrix upon formation, while coating REE are found in the authigenic Fe-Mn-rich particles, which attach onto the test surface after the organism dies; detrital REE originate from alumino-silicate detritus [*Palmer*, 1985]. It has long been hypothesized that the tests of sedimentary planktic foraminifera preserved ambient water signatures of the depth where they formed their calcite shells [e.g. *Vance and Burton*, 1999; *Burton and Vance*, 2000; *Vance et al.*, 2004]. However, it has now been established that in most cases these signals are overwritten as the tests sink down the water column. Once the tests are deposited at the seafloor, the planktic foraminifera represent primarily a bottom water signature [*Roberts et al.*, 2012; *Kraft et al.*, 2013; *Tachikawa et al.*, 2014; *Howe et al.*, 2016b]. The post-depositional surficial Fe-Mn oxyhydroxides that attach to the tests after they are deposited at the seafloor also represent bottom water seawater [*Palmer and*

Elderfield, 1985; *Rutberg et al.*, 2000; *Gutjahr et al.*, 2007]. Thus, assuming they have not been affected by pore water [e.g. *Tachikawa et al.*, 2014], the calcite tests and the Fe-Mn oxides – the non-detrital phases of authigenic tests – provide a great archive for ambient bottom water mass ε_{Nd}.

1.4 RESEARCH AND OBJECTIVES

This study assesses the ε_{Nd} systematics of sedimentary foraminifera samples of two gravity cores retrieved on the western margin of South Africa. One of the main goals of this study is to use the foraminiferal ε_{Nd} to reconstruct the ambient bottom water masses of the Holocene and LGM, and thus obtain a better understanding of the glacial-interglacial shifts of (regional) water masses in the Cape Basin. As previously mentioned, the oceanographic processes occurring in the southeast Atlantic are of great importance for the MOC and thus the global climate. The climatic changes during the last glacial weakened the leakage of subtropical Indian ocean water into the South Atlantic, which has been linked to the reduced formation of NADW [*Rutberg et al.*, 2000]. Paleoceanographic studies also suggest that water masses present in the Cape Basin at the time were more influence by southern sourced water masses than they are today and thus exhibited more radiogenic ε_{Nd} ratios (Figure 3) [*Howe et al.*, 2016c and references therein]. Rutberg et al. [2000] stressed the importance of further studying the ε_{Nd} of the region to track variations of the position of the Agulhas Retroflection as this would provide valuable information on the driving forces of the magnitude of the Agulhas over the last 20,000 years. They further stated that a detailed map of Nd isotopic ratios of the area would allow to systematically reconstruct changes of the Agulhas leakage. Since then, various studies have been conducted in the Cape Basin [*Piotrowski et al.*, 2012; *Howe et al.*, 2016c; *Wei et al.*, 2016]. Most recently, Howe et al. [2016c] carried out a comprehensive review of the available ε_{Nd} data from previous studies with new foraminifera data from the South Atlantic. As graphically depicted in Figure 3, the glacial foraminiferal ε_{Nd} data indicate that the southeastern Atlantic Ocean water masses had high ε_{Nd} (more radiogenic) during the LGM and then transitioned to lower ε_{Nd} ratios in the Holocene. The LGM data show a higher influence of Southern Component Water (SCW), which can be attributed to the northward expansion of the ACC during the last glacial [*Oppo and Fairbanks*, 1987; *Howe et*

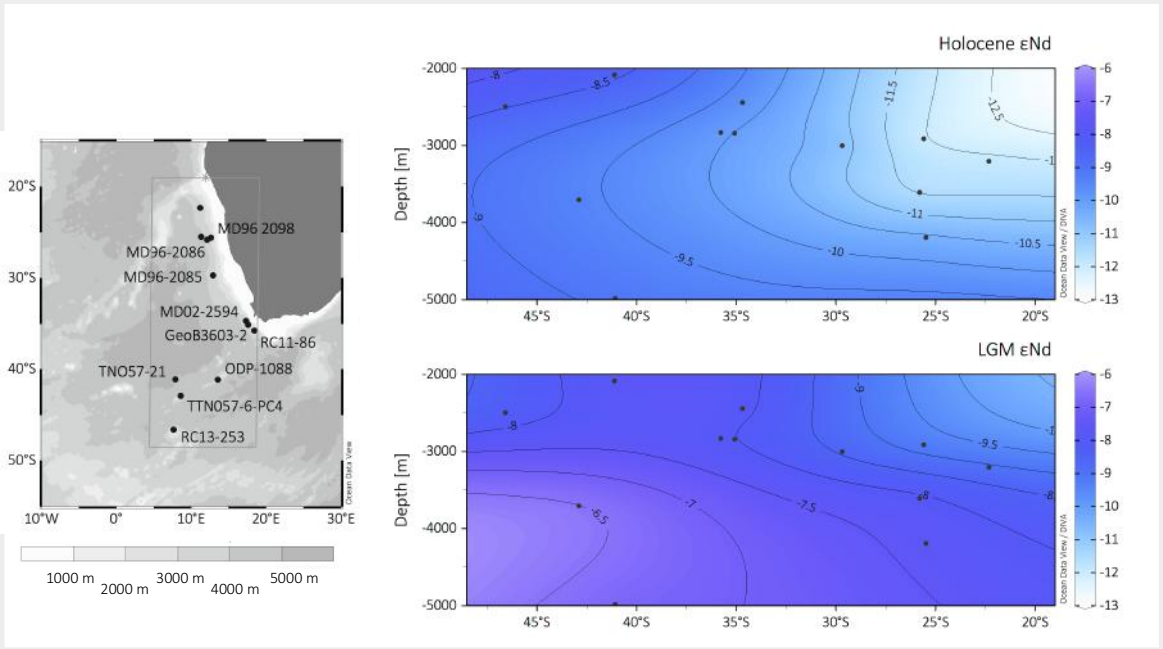

Figure 3. Holocene (top right) and LGM (23 to 18 ka) (bottom right) ε_{Nd} ratios of the southeast Atlantic region (2000 to 5000 meter below sea level (mbsl)) off the coast of southern Africa (19.0°S to 48.5°S) reconstructed using foraminifera ε_{Nd} data from previous sediment core studies. A map showing the sampling location of all cores included in the cross-section is depicted on the left. Core locations are indicated as black dots ("•") in the cross-sections on the right; a cross-section including station labels is presented in Appendix A: Data from previous studies

The map and cross-section graphics were created using the data presented in Appendix A: Data from previous studies [*Piotrowski et al.*, 2012; *Howe et al.*, 2016c, supplementary information; *Wei et al.*, 2016] with the visualization software Ocean Data View (ODV) [*Schlitzer*, 2017].

al., 2016c]. Modern day values of the area, on the other hand, are found in agreement with those of modern Eastern NADW (hereafter ENADW), and indicate that the modern Cape Basin water masses are more highly influenced by Northern Component Water [*Wei et al.*, 2016 and references therein]. These findings are further supported by $\delta^{13}C$ and Cd/Ca records [*Wei et al.*, 2016]. By measuring the Nd isotope composition, this study aims to further contribute to a high-resolution ε_{Nd} database for the southeast Atlantic. Since the southeast Atlantic is such an important area for the AMOC, attaining a better understanding of the paleoceanographic changes in the region is crucial for explaining the variations of the AMOC in the past. Therefore, a detailed ε_{Nd} database of the Cape Basin region in particular will allow the exact location of where the variations of the bottom water masses took place in the past.

To provide an even better understanding of the changes in water mass circulation, this study additionally analyzes foraminifera samples from marine isotope stage (MIS) 3. MIS3 was the interglacial period that preceded the LGM and is believed to have had a great influence on the further

development of the current interglacial stage [*Tzedakis et al.*, 2017]. MIS3 was cooler than the Holocene, yet warmer than MIS2, thus it is hypothesized that the water mass systematics during that period resembled those during the transition from the LGM to the Holocene (Termination I). Therefore, the data presented do not only allow tracing of the water masses over a greater temporal range, but may provide further information on the transition of the last glacial to the Holocene.

Finally, Nd stable isotope studies of sedimentary foraminifera tests have not been carried out at the University of Cape Town (UCT) before, so this study acts as a pilot project to find a suitable sample preparation procedure that can then be reproduced for the other gravity cores. This study aims to find a method that does not require a great amount of the sample as the sample availability is often limited. Both handpicked mixed foraminifera samples and bulk foraminifera samples are analyzed following the sample preparation procedure proposed by the Cambridge group [*Tachikawa et al.*, 2014], which provides a promising method for mixed species foraminifera. As previously pointed out, the ε_{Nd} ratio of sedimentary planktic and benthic foraminifera do not vary as both represent bottom water, thus bulk and planktic foraminifera are expected to exhibit similar ε_{Nd} systematics. Most preparation procedures suggest a minimum sample weight of 20 mg of planktic foraminifera [e.g. *Roberts et al.*, 2012; *Kraft et al.*, 2013; *Tachikawa et al.*, 2014], so, if proven to be a reliable proxy, bulk foraminifera could provide an alternative in the future if the amount of sample available is limited.

2 OCEANOGRAPHIC SETTING

2.1 BATHYMETRY

The opening of the South Atlantic Ocean started around 130 Ma ago in the early Cretaceous with the break-up of the supercontinent Gondwana [*Eagles*, 2007; *Torsvik et al.*, 2009], and was immediately followed by the formation of the western margin of southern Africa [*Eagles*, 2007]. The Cape Basin formed as a result of rifting of the passive western margin [*Nürnberg and Müller*, 1991; *Eagles*, 2007]. In the south, the Cape Basin is limited by the Agulhas Ridge, the marginal ridge of the northeast to southwest trending Agulhas fracture zone, which separates the ocean deep basins from the African continent (Figure 4) [*Rabinowitz*, 1976 and references therein; *Scrutton*, 1976]. To the northwest, it is bound by the Walvis Ridge, which formed as a results of hotspot volcanism [*Emery et al.*, 1975]. The Walvis ridge extends from the shallow Namibian coastal region to the Mid-Atlantic Ocean Ridge in the west, and limits the flow of deep water (>3000 m) from the Angola Basin into the Cape Basin [*Nelson and Hutchings*, 1983].

Figure 4 (next page). (a) Schematic map and (b) cross-section along 30°S showing the regional bathymetry and oceanographic setting around southern Africa. The locations of GeoB8336-6 and GeoB8342-6, the two gravity cores presented in this study, core MD96-2085 and that of the other cores discussed by Howe et al. [2016c] are indicated as described in the legend. Core MD96-2085 [*Howe et al.*, 2016c] was taken on the western continental slope as well (~3001 mbsl), and is later discussed in comparison to GeoB8336-6 and GeoB8342-6. The map illustrates major bathymetric features and schematically displays the regional modern upper ocean circulation and the deep water masses of interest; the light blue line indicates the location of the cross-section depicted below. The cross-section schematically shows the position of water masses in the Cape Basin as described in the literature.

AAIW extent of the Angola Basin is not true to scale (water depth); AAIW has a weak signature in the Angola Basin [*Stichel et al.*, 2012], thus the color scheme should be considered an indicator for where the water masses are more distinguishable.

Maps were created in ODV [*Schlitzer*, 2017] using the information provided by Diekmann & Kuhn [2002], Dingle et al. [1987], Lutjeharms & Stockton [1987], Peterson & Stramma [1991] and Stramma & England [1999]; core coordinates were given by Schneider et al. [2003] and Cheng et al. [2002a, 2002b]; ε_{Nd} data for the cross-section are derived from the references in the introduction and Stichel et al. [2012]

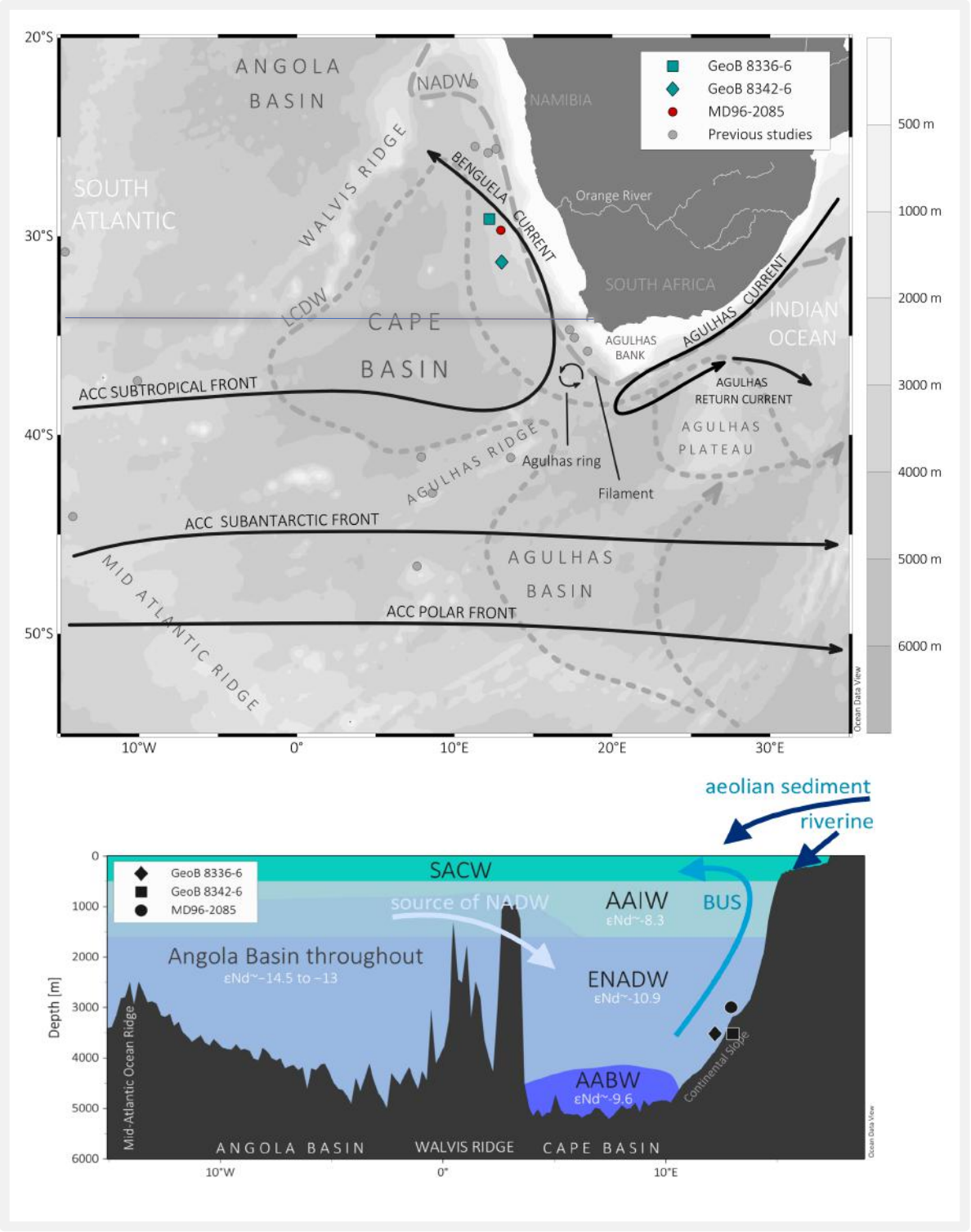

SEDIMENT TRANSPORT AND INPUT

Sediment transport in the study area (Figure 4) is believed to be dominated by the Benguela Current and the movement of AABW; the Benguela plays a major role in sediment generation but only a

minor role in sediment movement [*Dingle et al.*, 1987 and references therein]. The potential sediments that could enter the Cape Basin are glauconite, phosphorite, pelagic carbonate sand, opal, and fine terrigenous debris [*Dingle et al.*, 1987]. Terrigenous sediments from the African continent are transported to the Cape Basin by wind and through rivers. The aeolian sediments are picked up by the strong southeasterly trade winds (kabatic winds) and get carried to 200 km across the continental shelf [*Dingle et al.*, 1987]. The riverine sediment input is limited as only three of the rivers south of 22°S are perennial – the Orange, Olifants and Berg rivers. The Orange River has notably the highest annual mean runoff and transports ~5.1 million tons of mud sediment into the Cape Basin per year [*Dingle et al.*, 1987; *Compton et al.*, 2010]. Most of the discharged sediment is deposited near-shore, where it accumulates and forms the Namaqualand mudbelt [*Dingle et al.*, 1987 and references therein; *Herbert and Compton*, 2007]. Only a small amount of the mud is picked up by the Benguela Current and carried across the shelf to the Walvis Ridge and possibly beyond [*Dingle et al.*, 1987 and references therein]. The sediments found in the study region, the western continental slope, have variable riverine and aeolian influences [*Compton and Wiltshire*, 2009; *Compton et al.*, 2010]. The sediment is dominated by biogenic grains (calcareous nanoplankton and foraminifera) from the highly productive Benguela Upwelling System (see below), and are then deposited on the seafloor [*Schneider et al.*, 2003 and references therein].

2.2 OCEANOGRAPHIC SETTING

2.2.1 THE BENGUELA CURRENT AND THE BENGUELA UPWELLING SYSTEM (BUS)

The South Atlantic Current carries South Atlantic Central Water (SACW) from South America across the Atlantic. Off the west coast of southern Africa, SACW is picked up by the Benguela Current, which moves the cold saline water mass northward along the coastline. At the Angola-Benguela front, a convergence zone, the Benguela Current then deflects to the northwest and flows across the Atlantic towards the Brazilian shelf, closing the loop of the South Atlantic subtropical gyre [*Peterson and Stramma*, 1991; *Jansen et al.*, 1996; *Shannon and Nelson*, 1996; *Stramma and England*, 1999].

As the water flows along the west coast of southern Africa, the kabatic winds induce the upwelling of cold, nutrient-rich water [*Lutjeharms and Meeuwis*, 1987; *Shannon and Nelson*, 1996]. The Benguela upwelling system (BUS) is one of the most productive marine regions in the world [e.g. *Shillington*, 1998; *van der Lingen et al.*, 2006]. As upwelling occurs mostly in localized upwelling cells, the rates of upwelling vary greatly along the west coast. The most productive upwelling cell is the Lüderitz cell (~25°S), located off the coast of the town of Lüderitz, Namibia [*Lutjeharms and Meeuwis*, 1987].

2.2.2 THE AGULHAS CURRENT AND AGULHAS LEAKAGE

While other eastern boundary currents are commonly only bound by one warm water current on the equator side, the Benguela is also bordered by a tropical current to the south – the Agulhas Current [*Peterson and Stramma*, 1991; *Stramma and England*, 1999]. The Agulhas Current originates in the Indian Ocean and transports warm central waters from the Indian Ocean westwards along southeastern Africa. The exact cause of the Agulhas Current is not yet entirely understood, however, it is now commonly believed that its origin primarily lies in the Mozambique Current, the East Madagascar Current, Red and Arabian sea water, Indonesian through-flow water, and, most importantly, the subgyre recirculation [*Lutjeharms*, 2006; *Beal et al.*, 2011]. The current follows the coastline southwards and then circulates from the east around the southern tip of South Africa. The Agulhas Current "retroflects" between 16°E and 20°E, off the coast of Port Elizabeth and flows back as the Agulhas return current [*Lutjeharms and van Ballegooyen*, 1988; *Stramma and England*, 1999; *Lutjeharms and Ansorge*, 2001]. Not all water is returned into the Indian Ocean and some warm, salty Indian Ocean water is exported into the Atlantic as the Agulhas leakage. The strength of the Agulhas leakage is predominantly driven by the westerlies, the position of the ACC and Subtropical Front (STF) [*Beal et al.*, 2011; *Durgadoo et al.*, 2013].

2.3.3 DEEP AND INTERMEDIATE OCEAN CIRCULATION OF THE CAPE BASIN

The deep Cape Basin is filled with ENADW and AABW. AABW is commonly subdivided into two components: Lower Circumpolar Deep Water (LCDW), composed of old deep water masses, and the

denser Weddell Sea Deep Water (WSDW) [*Stramma and England*, 1999]. LCDW originates from the Antarctic Circumpolar Current (ACC), flows northwards through the Atlantic-Indian mid-ocean ridge and into the Agulhas Basin. After circulating the eastern and western Agulhas Basin, it either flows eastward or enters the Cape Basin at the northeastern Agulhas Ridge. Once in the Cape Basin, LCDW continues to rotate clockwise before also flowing further eastward into the Indian Ocean (Figure 4) [*Dingle et al.*, 1987; *Stramma and England*, 1999]. NADW enters the southeast Atlantic in the Angola Basin and then spills into the Cape Basin through the Walvis Ridge, where it flows over the denser Lower Circumpolar Deep Water (>4000 m) [*Dingle et al.*, 1987; *Schmiedl et al.*, 1997; *Stramma and England*, 1999 and references therein]. NADW is further controlled by the movement of Agulhas rings, which move through the Cape Basin, and induce an eddy thickness flux. This shifts the movement of NADW and forces the water mass to circulate through the Basin [*Beal et al.*, 2011; *van Sebille et al.*, 2012]. Cape Basin NADW is found as deep as 4000 mbsl, and is overlaid by AAIW (1600 to 500 mbsl), which forms the inner boarder between deep water and SACW [*Stichel et al.*, 2012].

3 MATERIAL AND METHODS

3.1 CORE SELECTION

For this study, the ε_{Nd} ratios of foraminifera were needed from at least two of the gravity cores retrieved from the Cape Basin during the first leg of the M57 research cruise (M57/1) of the RV Meteor in 2003 (Figure 5). To measure the variations between glacial and interglacial deep water masses, the cores had to be taken from the deep-water sites, and, to assure that reliable samples from the Holocene and LGM would be available, the top core sediment had to have remained unscathed during core retrieval. Finally, in order to assure that the ε_{Nd} measurements accurately represent ambient in-situ water masses, it was of great importance that the sediment of the cores had not been redeposited or reworked. While several core catcher samples taken on the shallower mudbelt sites indicated signs of sediment reworking, the cores taken in the deep ocean deep sites showed no evidence of reworking [*Schneider et al.*, 2003]. Therefore, after careful evaluation of the data and the descriptions of the cores available, it was decided that gravity cores GeoB8336-6 (29°12'58"S/12°20'64"E 3524 mbsl) and GeoB8342-6 (31°29'99"S/13°00'01"E, 3521 mbsl) from the northern deep ocean site on the western margin would be the best fit for the study.

During the on-board assessment, both cores had been laterally split in half, described (logged) and photographed, and using a hand-held spectrophotometer, the percent reflectance values of sediment color over the visible light range (400 nm to 700 nm) were taken. Sediment subsamples in two parallel series of syringe samples (10 cc) were extracted in 4 cm depth intervals; the Department of Geological Sciences at UCT houses one series of these samples. For the purpose of this study, the sand fraction

(>63 µm) of the gravity cores was samples, which had previously been processed and ultrasonically cleaned (Eugene Bergh, personal communication, February 2017).

A summary and schematic illustration of the lithostratigraphy in combination with the sediment reflectance (L*; 'lightness') profiles of the top meter of both cores can be found in Appendix A: Data from previous studies and reports.

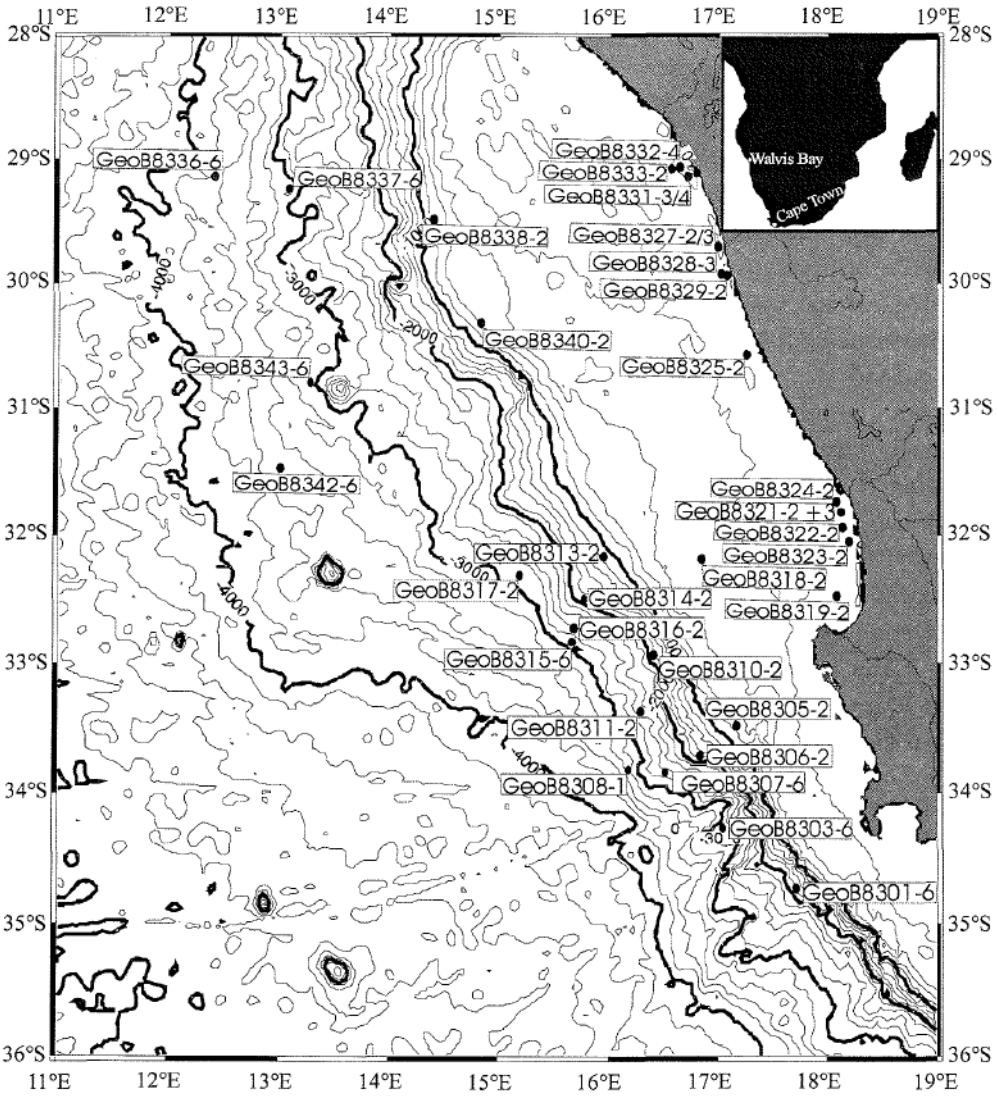

Figure 5. Bathymetric map showing the approximate location of the gravity cores retrieved during M57/1 (taken from Schneider et al. [2003].

3.2 FORAMINIFERA SAMPLE SELECTION

3.2.1 RARE EARTH ELEMENT CONCENTRATION PRE-MEASUREMENTS

As this was the first time that the Nd isotopic composition was measured on sedimentary foraminifera at UCT, the rare earth elements concentrations of bulk foraminifera samples from the core were measured to get a better estimate of what amount of sample would be needed. Therefore, ~9 to ~27 mg of bulk foraminifera from the 63 to 250 µm fraction were weighed out from all six core intervals of interest. To assure that there was no terrigenous sediment inside of the inner chambers of the tests, the sediment was placed into a clean glass petri dish and crushed using one glass slide. The test fragments were then transferred into a glass beaker with ~5 ml of 'ultra-pure' water and placed in an ultrasonic bath for one minute at a time. The water was pipetted to waste and the samples were ultrasonicated again until the water showed no more signs of impurities (clay). To further reduce the risk of contamination, the test fragments were then examined for included terrigenous particles under a binocular microscope; when present, these 'dirty' grains were carefully removed using a fine-haired brush.

The samples were then transferred into Teflon beakers. The test fragments were digested using 12M HCl in fume hoods without the addition of heat. Then, the samples were dried down on a hotplate. 3 ml of concentrated HNO_3 were added to remove the HCl, and the samples were again dried until they were completely dry. The samples were then diluted using 5% HNO_3 and ultrasonicated for one hour. Finally, the samples were diluted ~3500 times. The REE concentration measurements were then carried out on a ThermoFisher XSeries2 quadrupole intercoupled plasma mass spectrometer (ICP-MS) at UCT's Quadrupole ICP-MS facility using Argon as a carrier gas. To assure the accuracy of the measurements, In, Bi, Re and Rh were used as internal standards. The REE concentration measurements and PAAS-normalized values of the bulk foraminifera samples from the GeoB8336-6 and GeoB8342-6 are presented in Table 5 and Table 6 (Appendix C: REE pre-concentrations measurement data), respectively.

All samples exhibited overall low rare earth element concentrations; the concentrations of the samples from GeoB8336-6 were generally the highest. The Nd concentrations ranged from 1.6 ppm (R36/6b) to 2.8 ppm (R42/6c).

To assure that these Nd measurements represent the non-detrital REE concentrations of the foraminifera, which were needed for the Nd isotope analysis, the samples' concentration measurements were normalized to Post Archean Shale (PAAS; denoted with subscript 'SN'). REE_{SN} can provide a powerful tool for determining the origin of certain sediments [e.g. *Elderfield and Greaves*, 1982; *Bau and Dulski*, 1995; *Bau et al.*, 1996]. 'Pure' marine sediments that form from (modern) seawater, for instance, exhibit distinct trends and relative anomalies, such as negative Ce_{SN} anomalies and heavy-over-light REE_{SN} (HREE/LREE) enrichment, which resemble those of the REE_{SN} of modern seawater [*Elderfield and Greaves*, 1982; *Bau et al.*, 1996]. In comparison, terrigenous sediments commonly show flat shale-normalized patterns [*Cruse et al.*, 2000].

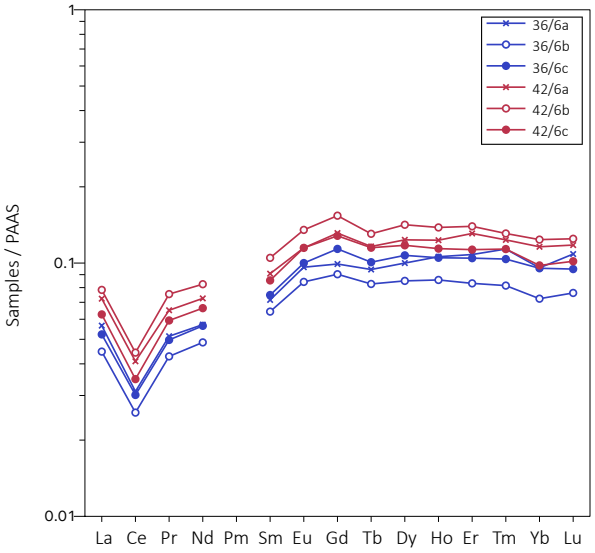

Figure 7. Post-Archean shale-normalized REE signatures of bulk foraminifera samples from cores GeoB8336-6 (R36/6a-c) and GeoB8342-6 (R42/6a-c). This plot was created using the plotting and visualization software Abscissa [*Brühl*, 2015].

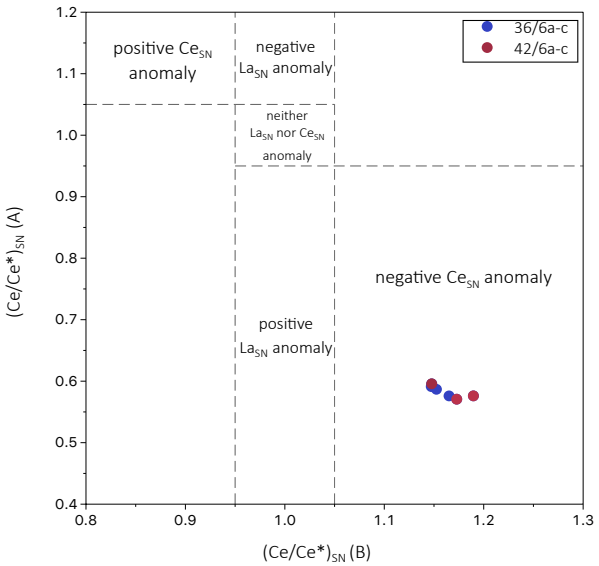

Figure 7. vs. $(Ce/Ce^*)B_{SN}$ ratios of bulk foraminifera samples from cores GeoB8336-6 (R36/6a-c) and GeoB8342-6 (R42/6a-c) to visualize possible Ce_{SN} and La_{SN}. All samples exhibit no La_{SN} and significant Ce_{SN} anomalies. This plot was created after Bau & Dulski [1996] using Abscissa [*Brühl*, 2015].

All samples presented in this study exhibited similar subparallel REE_{SN} signatures (Figure 7). Anomalies were calculated using the formulas provided by Bau & Dulski [1996], Bolhar et al. [2004] and Martin et al. [2010] (Table 7; Appendix C: REE pre-concentrations measurement data).

The samples exhibit distinct negative relative Ce_{SN} anomalies ($Ce/Ce^*_{SN}A$ ~ 0.65 to 0.71/ $Ce/Ce^*_{SN}B$ ~ 0.57 to 0.60) (Figure 7), significant positive relative Gd_{SN} anomalies (Gd/Gd^*_{SN} ~ 1.12 to 1.29). Further, all samples exhibit light REE_{SN} (LREE) to heavy REE_{SN} (HREE) depletion ($(Pr/Yb)_{SN}$ ~ 0.52 to 0.61). These anomalies are commonly found in marine sediments and are in agreement with those previously reported for foraminifera [*Martin et al.*, 2010]. Finally, all samples also show relative medium REE ($MREE/MREE^*_{SN}$ ~ 1.22 to 1.45) over LREE and HREE. $MREE_{SN}$ enrichment is typical for hydrogenous Fe-Mn oxides [*Martin et al.*, 2010 and references therein]. As 90% of the rare earth elements of non-detrital foraminifera are found in the diagenetic coatings [*Palmer*, 1985], this enhancement is to be expected in foraminifera samples. These findings strongly suggest that the detrital REE were removed prior to the analysis, and that the Nd concentrations measured represent only those of the non-detrital fraction of the tests. The sample Nd concentrations lie within the range of those of foraminifera previously analyzed for Nd isotope concentrations [e.g. *Kraft et al.*, 2013]. Thus, the Nd isotopes of the samples considered in this study should be well detectable when prepared the same way as foraminifera from previous studies.

3.2.2 FORAMINIFERA SELECTION

For the Nd isotope analyses, planktic foraminifera tests from the sand fraction were taken at core depth intervals 8/9 cm (N36/6a), 27/28 cm (N36/6b) and 60/61 cm (N36/6c) for GeoB8336-6, and 16/17 cm, 40/41 cm (N42/6b) and 68/69 cm (N42/6c) for GeoB8342-6. As later explained in 5.1 Age model, these depths were selected based on the cores L* profiles in correlation to other cores from the region and are thought to represent the marine isotope stages (MIS) 1 (Holocene), MIS2 (the LGM) and MIS3, respectively. The high abundance of foraminifera in the 16/17 cm depth interval of GeoB8342-6 allowed for a split sample, N42/6a I and N42/6a II. To reliably examine the exact extent of the regional water masses during the LGM and Holocene, the tests' ε_{Nd} must accurately represent the Nd isotope composition of the ambient in-situ bottom water masses. Therefore, the test selection focused on reducing the risk of selecting redeposited or reworked sediment. As previously mentioned, the broad inspection of the cores found that both gravity cores contained no indications that any shell

debris from previous rocks units had been reworked, nor transported down the slope [*Schneider et al.*, 2003]. However, to further reduce the risk of impurities, only undamaged, whole tests were picked. The handpicked mixed samples were predominantly composed of *Globorotalia inflata., Neogloboquadrina pachyderma* and *Orbulina universa.* Further, bulk foraminifera samples from the 63-250 µm fraction were taken at 60/61 cm (GeoB8336-6; N36/6c bulk) and 68/69 cm (GeoB8342-6; N42/6c bulk). The sample weights, descriptions as well as pictures of the samples are presented in Appendix B: .

The samples were then mechanically processed following the same procedure that was used for the rare earth element samples. Despite the repeated ultrasonication, some of the tests were still covered and/or filled with pale yellow to brown coatings and fillings. Some tests also exhibited black coatings, which are most likely manganese oxides (Figure 8). Further ultrasonication was conducted to attempt the removal of the coatings, however, they appeared to be incorporated into re-precipitated calcite and remained on the samples. The crushed foraminifera tests were then weighted out and added to a 15 ml acid cleaned centrifuge.

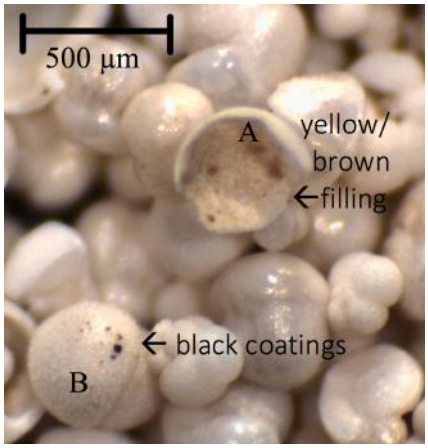

Figure 8. Foraminifera tests from sample 'N36/6c bulk'. Broken *Orbulina universa* test filled with calcified mud (A) and *Globorotalia inflata* with dark Mn coatings (B).

3.3 WET GEOCHEMISTRY

3.3.1 SAMPLE PREPARATION FOR ND ISOTOPE MEASUREMENTS

RECOMMENDATIONS FROM PREVIOUS STUDIES

According to Tachikawa et al. [2014], the success of the sample preparation method primarily depends on the foraminiferal calcite content and the type, volume and concentration of the acid used to dissolve the foraminifera. They further stressed the significance of using one consistent sample preparation method for all foraminiferal ε_{Nd} studies to assure the consistency of the results from different studies. In the past, the importance of using cleaned foraminifera, i.e. foraminifera that were

not only cleaned mechanically ('uncleaned') but also had the authigenic phases chemically removed, was commonly recommended as it was believed that cleaned sedimentary planktic foraminifera represented surface ε_{Nd} ratios [e.g. *Vance and Burton*, 1999; *Burton and Vance*, 2000]. However, a comprehensive report [*Tachikawa et al.*, 2014] compared the effects of various cleaning methods on the Nd isotope composition [*Burton and Vance*, 2000; *Vance et al.*, 2004; *Roberts et al.*, 2010; *Elmore et al.*, 2011; *Piotrowski et al.*, 2012; *Kraft et al.*, 2013] and concluded that, while the overall neodymium content of sedimentary foraminifera is reduced during the chemical cleaning process, 'cleaned' foraminifera exhibit the same Nd isotope compositions (within analytical error) as those foraminifera that were solely mechanically cleaned.

SAMPLE PROCEDURE USED IN THIS STUDY

The samples were prepared for the wet geochemistry processing by following the protocol presented by the Cambridge group (Tachikawa et al. [2014], after Elderfield et al. [2012] , Piotrowski et al. [2012], Roberts et al. [2010] and Roberts et al. [2012]), a preparation procedure created to extract "bottom water ε_{Nd} values from" planktic foraminifera. The method is suitable for both (chemically) 'cleaned' and 'uncleaned' tests [*Tachikawa et al.*, 2014], however, as the Nd concentrations are reduced during chemical cleaning and the foraminifera abundances in some of the GeoB samples were low, the tests were left 'uncleaned' to assure that the Nd concentrations would be high enough to be detectable by the Multicollector ICP-MS.

In a clean lab environment, the fragments were covered in 500 µl 'ultrapure' water. Then, to dissolve the fragments, up to 10 aliquots of 100 µl of 1 M acetic acid (max. 1 ml total) were added to the tube, and left to react after each aliquot until the fragments no longer reacted with the acid (bubbling subsided), which typically took 1 to 2 hours; once the samples are fully dissolved, no further acid should be added. By adding the acid in small aliquots and letting it dissolve in the smallest and lowest concentration possible, the method decreases the risk of leaching of terrigenous matter, which might otherwise be overlooked. The samples were still not dissolved after adding a total of 1 ml, thus, as suggest by the protocol, they were ultrasonicated for 10 minutes. After the ultrasonication was completed, the samples were left to react again until no more bubbles were present. At this stage,

most samples no longer contained any white test fragments; the foraminifera were fully dissolved. The samples were then centrifuged for 10 min at 4500 rpm to separate the terrigenous sediment from the samples, transferred into 1.5 ml acid cleaned centrifuge tubes, and centrifuged again for another 10 min at 10,000 rpm. The supernatants were transferred into acid cleaned Teflon vials and left to dry over night at 60°C. The dried samples were re-dissolved in nitric acid for one hour in order to attack organics and enhance the column chemistry [*Tachikawa et al.*, 2014]. The samples were again dried and redissolved, and then the Nd was sequentially separated following the chemistry presented by Miková [2007] [after Pin & Zalduegui [1997] and Pin et al. [1994]].

3.3.2 WET GEOCHEMISTRY: REFERENCES AND MEASUREMENTS

The Nd isotope measurements were carried out using a NuPlasma HR multi-collector ICP-MS (MC-ICP-MS) facility housed in the UCT Department of Geological Sciences. Following the standard procedure of the facility, the samples' Nd isotopes were analyzed as 50 ppb 2% HNO_3 solutions using a Nu Instruments DSN-100 Desolvating Nebulizer. To assure the accuracy of the measurements, JNdi-1, an international neodymium isotope reference standard similar to La Jolla Nd by Tanaka et al. with reported $^{143}Nd/^{144}Nd = 0.512115$ [2000], was used to bracket the samples; JNdi-1 was run before every six samples, which allowed for recalibration and, if needed, the correction of the sample measurements. The sample measurements were corrected for any Sm and Ce interference by measuring the ^{147}Sm and ^{140}Ce signals and the natural Sm and Ce abundances. Further, instrumental mass fractional was corrected using the exponential law and a $^{146}Nd/^{144}Nd$ value of 0.7219.

In addition, ~25.03 mg of the UCT internal carbonate standard, Namaqualand marble (NM95), was weighted out and prepared and analyzed the same way as the samples. NM95 has never before been analyzed for its Nd isotope composition, thus no reported data are available. Split samples N42/6a I and N42/6a II show identical ε_{Nd} ratios within error (~-10.0±0.4 and ~-10.4±4, respectively), which supports the reproducibility of the sample measurements (Appendix D: Nd isotope measurement data, Table 8).

4 RESULTS

An overview of the Nd isotope data of all samples can be found in Table 8 (Appendix D). ε_{Nd} ratios of the samples were calculated using the equation provided by Jacobsen & Wasserburg [1980].

The samples exhibited $^{143}Nd/^{144}Nd$ ratios ranging from 0.512087±0.000017 (N36/6a) to 0.512241±000014 (N42/6b) with corresponding ε_{Nd} ratios of -10.7±0.3 to -7.7±0.3. Overall, both cores exhibit similar ε_{Nd} ratios for their respective 'a', 'b' and 'c' sample intervals (Figure 9). The cores' 'a' samples yield the lowest ε_{Nd} ratios, which range from $\varepsilon_{Nd(N36/6a)} = -10.7\pm0.3$ to $\varepsilon_{Nd(N42/6a\ I)} = -10.0\pm0.4$. N36/6b and N42/6b show the most radiogenic ε_{Nd} ratios ($\varepsilon_{Nd\ (N36/6b)} = -8.1\pm0.3$ and $\varepsilon_{Nd\ (N42/6b)} = -7.7\pm0.3$). The 'c' samples' Nd isotope composition is less radiogenic than that of the 'b' samples but the ε_{Nd} ratios are significantly higher than those of the samples N36/6a, N42/6a I and 42/6a II. N36/6c and N42/6c exhibit ε_{Nd} ratios of -8.8±0.3 and -8.6±0.4, respectively, which are identical within error to those of their accompanying bulk samples ($\varepsilon_{Nd\ (N36/6c\ bulk)} = -8.7\pm0.3$, and $\varepsilon_{Nd\ (N42/6c\ bulk)} = -8.8\pm0.3$).

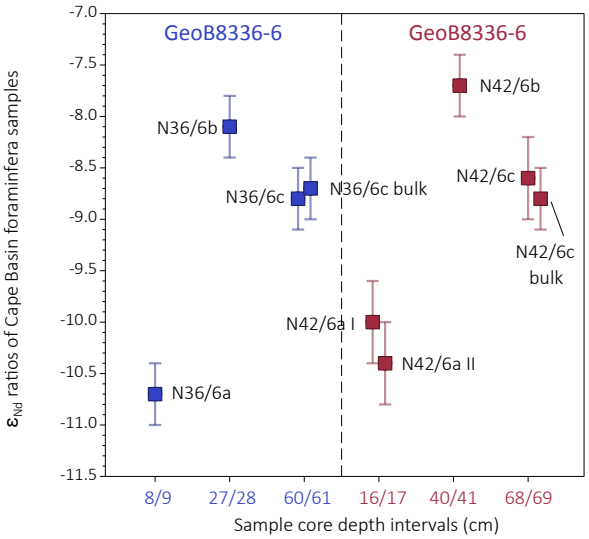

Figure 9. ε_{Nd} ratios of Cape Basin foraminifera samples from sediment cores GeoB8336-6 (blue) and GeoB8342-6 (red). 2σ external errors are indicated with error bars.

Graphic created in Abscissa [*Brühl*, 2015] with the Nd isotope composition measurement data provided in Table 8 in Appendix D: Nd isotope measurement data.

5 DISCUSSION

5.1 AGE MODEL

Most sediment cores today are dated based on using $\delta^{18}O$ and radiocarbon isotopes. Oxygen isotope and/or radiocarbon age records of GeoB8336-6 and GeoB8342-6 are not available to date. Therefore, tentative downcore 'Holocene' and 'LGM' depth intervals were identified based on the variations in the cores' sediment color reflectance (L*) records, the magnetic susceptibility profile of GeoB8336-6 and variations in both cores' foraminifera fauna, in correlation to the $\delta^{18}O$ and radio carbon age model provided for sediment core MD96-2085. MD96-2085 was retrieved from the Cape Basin in close proximity to the cores considered for this study (30°S, 13°E, 3001 mbsl), and has previously been dated using $\delta^{18}O$ systematics [Chen et al. 2002a, in supplement to Chen et al. 2002b]; the age model provided is based on the benthic foraminifera $\delta^{18}O$ Plio-Pleistocene stack (and $\delta^{13}C$ data) presented by Lisiecki and Raymo [2005].

Previous comparisons of L* profiles to $\delta^{18}O$ profiles have shown that distinct changes occur at the same depths in both profiles [*Schneider et al.*, 2003; *Compton and Wiltshire*, 2009]. These notable variations in the downcore L* profiles ('marker events') can be correlated to different marine isotope stages (MIS) [e.g. *Lisiecki and Raymo*, 2005], which were identified in previous studies. In combination with other core properties and the correlation to other (dated) cores, the L* profile may be a good indicator to preliminarily assess the core age [*Schneider et al.*, 2003; *Compton and Wiltshire*, 2009]. In addition to the L* profile, a magnetic susceptibility (κ) profile was created for GeoB8336-6. Like the evaluation of the sediment reflectance profile, κ profiles exhibit distinct pattern changes that also indicate changes with regards to the glacial and interglacial cycles. The magnetic

susceptibility is a measurement indicating how 'magnetizable' the sediment is, which, in most cases, is determined by the amount of ferromagnetic minerals present. Lithogenic compounds or sediment with high Fe (bio) mineralization exhibit a high magnetic susceptibility, while carbonate and silicate minerals show the lowest κ values [*Schneider et al.*, 2003 and references therein]. Upwelling and carbonate dissolution rates vary throughout the glacial-interglacial cycles, which is reflected in distinct changes in the κ profile of GeoB8336-6. The relative smoothness of the κ curve can be attributed to the fact that the measurements were taken non-linearly over intervals of 8 to 10 cm [*Schneider et al.*, 2003]. The discrete excursions noted in the L* profiles of both cores correlate to those found in the magnetostratigraphy of GeoB8336-6, and support the reliability of the indicative character of L*.

The marker events are further supported by distinct down-core changes in foraminifera abundances and/or fauna (Eugene Bergh, personal communication, November 2016/March 2017): the most abundant foraminifera species in both cores is *Globorotalia inflata,* a temperate water species [*Schneider et al.*, 2003]. In GeoB8336-6, *G. inflata* tests are far more common in the samples N36/6a and N36/6b, while *O. universa* were rare in those samples, but plentiful in N36/6c. Similar trends were reported for GeoB8342-6, however, the changes were not as pronounced as in GeoB8336-6. *N. duterei*, a warm water indicator species, is present at the 8/9 cm (N36/6a) sample depth, but absent from samples N36/6b and N36/6c. *Gs. Sacculifer* abundances exhibit similar trends: the warm water species is more commonly found in the upper sample than the intermediate sample depth. Specimen of *Neogloboquadrina pachyderma,* a cold-water species, on the other hand, are more abundant in N36/6b than in N36/6a. These changes of abundance of the indicator species are found to be in good agreement with the oceanographic setting proposed for the respective time periods. In GeoB8342-6, a notable decrease of left-coiling *Neogloboquadrina pachyderma* occurs between the two older sample intervals and that of MIS1. *N. pachyderma* is commonly found in polar to transition water ([*Rau et al.*, 2002]. This is in agreement with the findings from paleoceanographic studies, which suggest that the influence of polar water on the water masses in the Cape Basin was greater during the glacial period than today. *Globigerina bulloides* abundances are used to indicate productivity and

show an increase in the sample interval of MIS1 in comparison to the deeper samples [*Gordon et al.*, 1992]. The higher presence of the tropical/subtropical *Globigerinoides ruber* (alba), as observed in the top core samples of GeoB8342-6, has been linked to the growing influence of tropical Agulhas Current water in the past [*Rau et al.*, 2002]. Notable reductions of the tropical/subtropical species during the LGM suggest a reduction of the Agulhas leakage [e.g. *Rau et al.*, 2002; *Franzese et al.*, 2006], however, these changes in species abundances may also be attributed to various other factors [*Franzese et al.*, 2006 and references therein] and should thus not be considered a primary indicator for determining shifts in the water masses.

Altogether, however, the combination of the L* profiles and magnetic susceptibility systematics with the foraminifera abundances provide a good indication for the depths of MIS1 to 3. As graphically depicted in Figure 10, the cores could therefore be correlated to the $\delta^{18}O$ and radiocarbon data of MD96-2085. L* 1 and L*2 are believed to correlate to the maxima of MIS stage 1 and 3. 'Peak' MIS1 represents the Holocene Climatic Optimum, which took place approximately 9 to 8 thousand years ago in southwest Africa [*Gingele*, 1996]. The 'LGM' depth is identified where the discrete excursion between peak 1 and 2 lies. The exact depths of the first two L* 'peaks', as well as the sample intervals, are listed in Table 1 below.

Table 1. Overview of the sampling depths of the two sediment cores examined in this study [*Schneider et al.*, 2003]. The preliminary age model of the sample depths was established based on the correlation of the two cores to other cores as described in the text. As described and explained in the text, 'a', 'b' and 'c' samples represent the Holocene climatic maximum, the LGM and the climate optimum of MIS3, respectively.

				L*peak (cm)		**Sample interval depth** (cm)		
Core	**Latitude**	**Longitude**	**Depth** (mbsl)	L*1	L*2	'a'	'b'	'c'
GeoB8336-6	29°12.58 S	12°20.64 E	3524	11	61	8/9	27/28	60/61
GeoB8342-6	31°29.99 S	13°00.01 E	3521	17	67	16/17	40/41	68/69

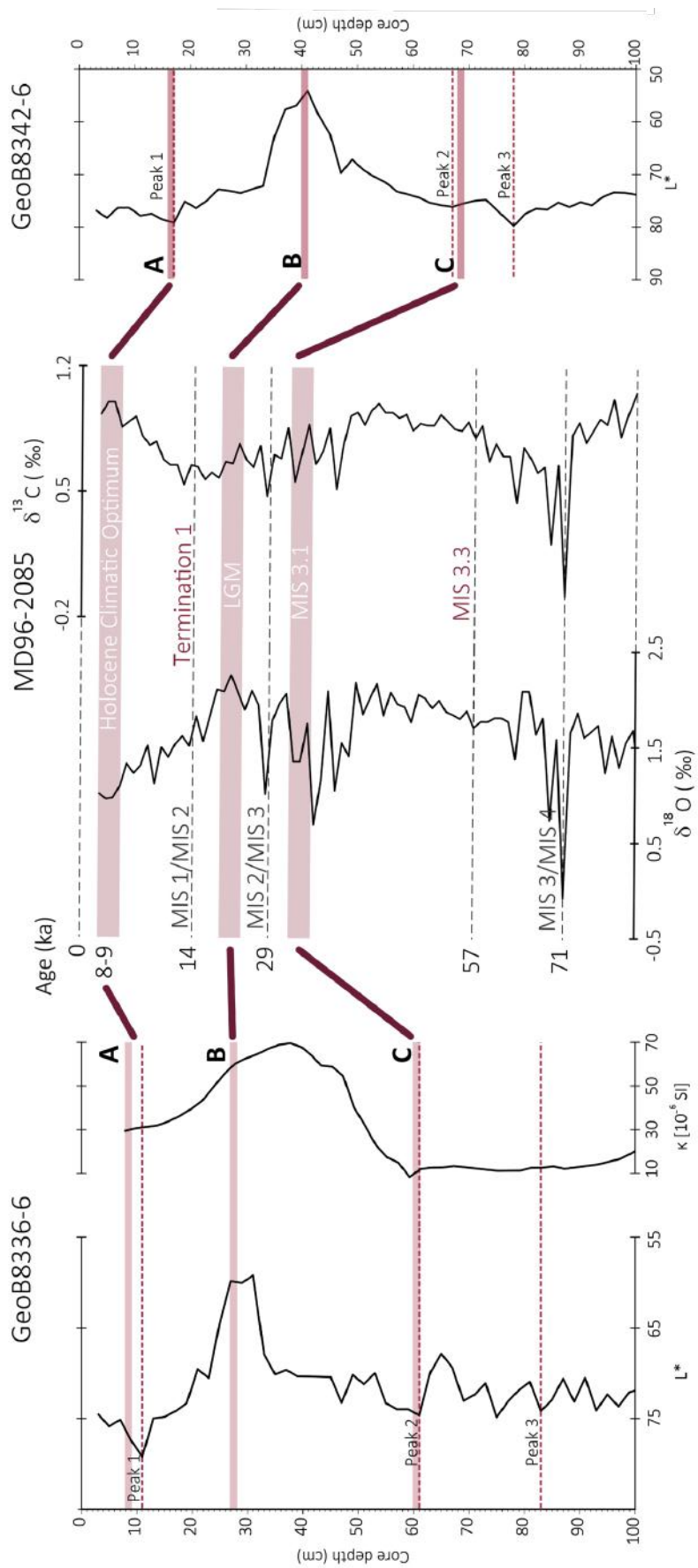

Figure 10. L* profiles of GeoB8336-6 and GeoB8342-6, and magnetic susceptibility profile (κ) (10^{-6} SI) of GeoB8336-6, correlated to core the delta-18-O and delta-13-C record from MD96-2085. Age model based on the delta-O-18 stack provided by Lisiecki and Raymo [2005]. Holocene Climate Optimum range for the southwest Africa taken from Gingele [1996]. The sample intervals are denoted 'A', 'B', 'C' as described in the text, and refer to MIS1, the LGM, and MIS3, respectively(graphs created in Abscissa [Brühl, 2015] using the data provided by Schneider [2003a, 2003b] and Cheng et al.[2002a in supplement to 2002b]

5.2 EVALUATION OF THE SAMPLES AND SAMPLE PREPARATION METHOD

As expected, the sample preparation protocol provided by the Cambridge group proved to be a good preparation procedure. All terrigenous particles incorporated into the crystalline calcite on the tests that could not be removed mechanically separated from the tests during the wet chemistry preparation and were then separated from the 'pure' samples during centrifugation. Despite the low sample weights of some samples (~20 mg), the Nd concentrations were high enough to reliably detect the Nd isotope composition of all samples. The ε_{Nd} ratios of the two split samples, N42/6a I and N42/6a II, show the same values within the range of the instrumental error ($\varepsilon_{Nd\ (N42/2a\ I)}$ = -10.0±0.4 and $\varepsilon_{Nd\ (N42/2a\ I)}$ = -10.4±0.4), which implies the reproducibility of our samples.

ND ISOTOPE COMPOSITIONS OF BULK FORAMINIFERA

As previously mentioned, benthic and sedimentary planktic foraminifera both acquire the Nd isotope composition of ambient bottom water, which implies that these ε_{Nd} could also be derived from non-selective bulk foraminifera samples. The Cambridge group's preparation procedure was initially created for planktic foraminifera, however, it also worked well for preparing the bulk samples so that the results of this study suggest that the protocol may also be used for the preparation of the latter. As previously explained, the bulk samples were taken non-selectively and thus included a mix of benthic and planktic sedimentary foraminifera. Since both attain bottom water signatures post deposition, they are expected to have similar ε_{Nd} ratios. As shown in Results, no significant variations were noted between the ε_{Nd} ratios of bulk samples and the mixed planktic foraminifera samples from the '-c' sampling depth. This suggests that both handpicked and (non-species selective) bulk sedimentary foraminifera represent ambient bottom water. Thus, if sediment is limited, bulk foraminifera samples could provide an efficient method for the reconstruction of ambient seawater ε_{Nd}. However, further studies should be carried out to support this assumption as the 'non-selective' bulk samples generally contained minor amounts of benthic foraminifera. This is because the benthic foraminifera abundances were generally very low in the deep-site M57/1 GeoB sediment cores (<1% of the total counts) [*Schneider et al.*, 2003]. Further, the samples were taken from the 63-250 µm size fraction;

most benthic foraminifera are larger than planktic foraminifera, therefore the size fraction could have added further bias towards the dominance of ε_{Nd} signals from planktic foraminifera.

It is also important to note again that the foraminifera of the sediment cores analyzed in this study showed no signs of reworking or downslope postdepositional transport. As previously explained, reworked and redeposited foraminifera do not represent the water of the sampling site and cannot be considered a reliable proxy for the reconstruction of ambient regional water masses. Therefore, if reworking or redeposition are thought to have occurred within the sampling region, handpicking the tests and only choosing those species and specimen that are most likely to be in-situ, i.e. are not allogenic or reworked, remains important. This is especially important in very dynamic areas such as near the shelf or slope [*Compton and Wiltshire*, 2009].

RECOMMENDATIONS FOR FUTURE FORAMINIFERAL ND ISOTOPE STUDIES AT UCT

Overall, the protocol provided by the Cambridge group proved to be a reliable sample preparation method, not only for planktic but also for bulk foraminifera samples. Therefore, the chemistry proposed in this procedure should be used for all future foraminiferal Nd isotope studies at UCT without alterations. However, as most samples only properly dissolved once placed into an ultrasonicated bath, two recommendations are made about the method. Firstly, to enhance the sample digestion process, it is recommended that samples be placed in an ultrasonic bath for 10 minutes if needed. The sample preparation method suggests that, if the samples are still not dissolved after adding a total of 1 ml of acetic acid, 'brief' ultrasonication can be applied to help digest the samples, however, the protocol does not further specify for how long they should be ultrasonicated for. Notable results were achieved after ultrasonicating the samples for 10 minutes; all samples were at least mostly, if not entirely, dissolved. Secondly, if the samples are only barely dissolved after adding the fifth aliquot of acid or do not appear to be reacting with the acid as a mud layer formed on top, we suggest that the samples could already be ultrasonicated after addition of the fifth aliquot to help the digestion. During the digestion process, the mud that was cemented onto some of the tests separated from the calcite and formed a layer on top of the undissolved sediment. This hindered the remaining sediment from reacting with the acid so that, even after the addition of all 10 aliquots of acetic acid,

the samples were still for the most part not dissolved. As previously mentioned, using one single sample preparation method throughout all foraminiferal ε_{Nd} studies is important to assure the consistency of the results, which is needed to create a comparable database. Ultrasonication is a purely mechanical process thus ultrasonicating the samples after the addition of the fifth aliquot of acid would enhance the digestion process and should not cause any inconsistencies in the chemical measurements; cross-study consistency in the Nd isotope composition measurements should therefore still be expected.

5.3 CAPE BASIN FORAMINIFERA AS A PROXY FOR AMBIENT BOTTOM WATER

As shown in 5.1, the age model used in this study provides a good preliminary framework to tentatively date the sediment cores and extract foraminifera samples from the marine isotope stages 1 to 3. Therefore, if the foraminifera tests analyzed in this study prove to be representative of ambient in-situ bottom water, they accurately represent the ancient Cape Basin bottom water masses and can be used as a regional bottom water proxy for MIS1, MIS2 and MIS3. To assure that the tests represent in-situ ambient seawater, the foraminifera samples must not have been reworked or deposited from shallower water depths. In addition to this, a good proxy may not exhibit any signs of contamination of detrital particles, either directly or through pore water, which is particularly common in areas where advection of volcanogenic material occurs or unradiogenic glacial flour is present [*Tachikawa et al.*, 2014].

As previously mentioned, all visible terrigenous matter present was removed from the tests either before or during the sample digestion. The ε_{Nd} ratios were further evaluated to assure they did not acquire detrital signatures through pore water, which would change the ε_{Nd} ratios of the samples notably. Basalt from the Walvis Ridge, one of the possible contaminants, exhibits ε_{Nd} ~-1 [*Richardson et al.*, 1982], i.e. values close to CHUR, so that contamination by matter from the ridge would greatly increase the ε_{Nd} ratios of the samples. Regional glacial flour, on the other hand, represents Archean ε_{Nd} ratios, and has significantly lower ε_{Nd} ratios (ε_{Nd} ~-24 to -37) [*Hemming*, 2004; *Piotrowski et al.*, 2008] than the measured ratios. A comparison to ε_{Nd} data from the literature showed that the ε_{Nd} ratios

presented in this study were found to be in good agreement with the regional Nd data reported for all three time periods (Figure 11): the ε_{Nd} ratios of 'a' and 'b' samples lie well within range of reported regional Holocene and LGM water mass ratios [*Piotrowski et al.*, 2012; *Howe et al.*, 2016c; *Wei et al.*, 2016], while ε_{Nd} ratios of 'c' samples are found in good agreement with Nd isotope data from MIS3 [e.g. *Rutberg et al.*, 2000; *Piotrowski et al.*, 2005]. Therefore, it can be assumed that the foraminifera tests analyzed in this study were not affected by any pore water contamination and that the samples accurately represent ε_{Nd} of ambient bottom water masses, making them a great proxy for regional ambient bottom water masses.

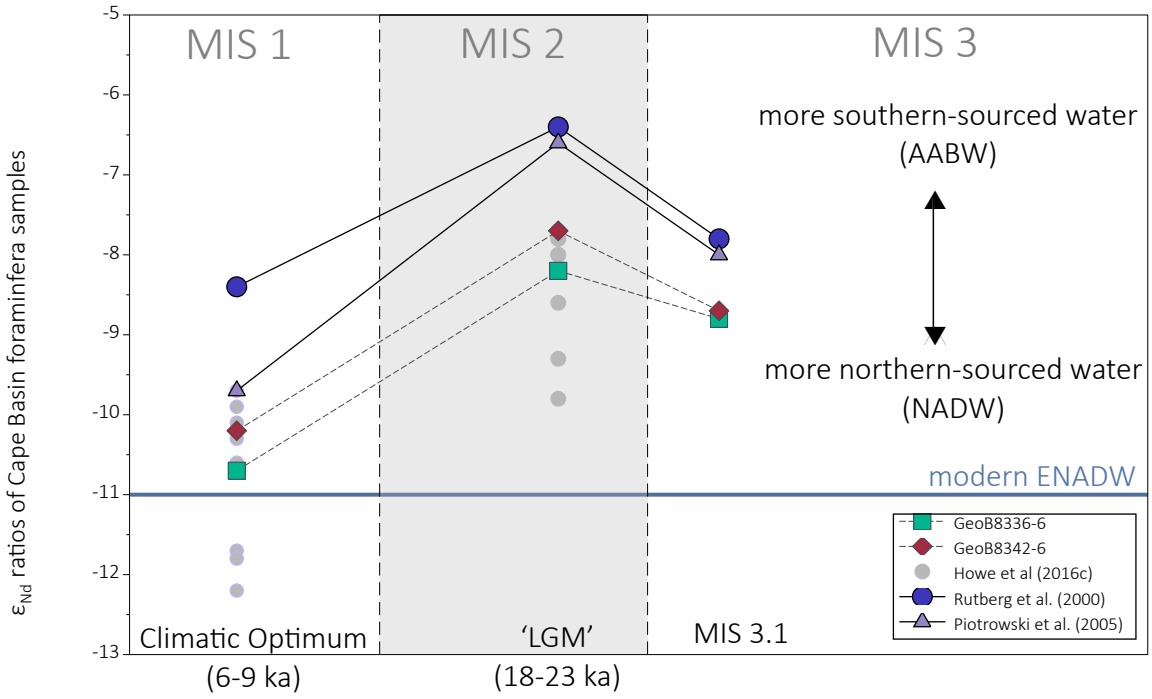

Figure 11. Graph showing the ε_{Nd} ratios of 'a', 'b' and 'c' samples of GeoB8836-6 '(▣')' and GeoB8342-6 ('♦'), and ε_{Nd} ratios of sediment cores from previous studies since MIS2 ('•') [Howe et al., 2016c, and references therein], and Rutberg et al. [2000] and Piotrowski [2005]. The different studies identified varying age intervals for the respective glacial-interglacial events, thus, to better visualize the results, the different study ages were combined as "intervals". The LGM was identified between 18 and 23 ka, and the Holocene Climatic Optimum (here denoted as 'Climatic Optimum', is shown from 6 to 9 ka. MIS3.1 were taken from ~36 ka [Rutberg et al., 2000] and ~38 ka [Piotrowski et al., 2005].

The maps were created in Abscissa [Brühl, 2015] using the data provided in this study (Appendix D: Nd isotope measurement data, Table 8) and the studies mentioned in the text; whenever more than one ratio was per sample available (N36/6c, N42/6a, N42/6c), the mean was used.

5.4 VARIATIONS OF CAPE BASIN WATER MASSES SINCE MIS3

5.4.1 THE EVOLUTION OF CAPE BASIN WATER MASSES AND CLIMATE SINCE THE LATE MIS3

Marine isotope stage 3, the interglacial period that preceded the LGM, was characterized by the occurrence of frequent Dansgaard-Oeschger events, phases of rapid warming. Modelling studies further suggest that the climate was generally warmer than the subsequent MIS2 [*Van Meerbeeck et al.*, 2008 and references therein]: Cape Basin sea surface temperatures (SST) are estimated around 14.25±1.75°C [*Sachs et al.*, 2001]. In comparison, the southeastern Atlantic SST during MIS2 and the transition to the warmer MIS1 is projected to lie somewhere between 13.5° and 19°C [*Sachs et al.*, 2001]. Before entering the cooling phase of the LGM, millennial-scale warming of 1° to 3°C took place (41 to 25 ka), which was most likely a result of increasing low-latitudinal solar radiation due to global obliquity variation cycles. The ε_{Nd} ratios of this warming period ($\varepsilon_{Nd(N36/6c/42/6c\ bulk)}$ = -8.8±0.4 to $\varepsilon_{Nd(N42/6c)}$ = -8.6±0.3) are more radiogenic than those of modern ENADW (ε_{Nd} = -10.9±1.2), which indicates that the Cape Basin water masses were influenced by southern sources; the influence was larger than during the Holocene, it was not as high as during the LGM.

A reduction of atmospherical CO_2 concentrations, lower northern summer insulations and the decrease in tropical Pacific SST eventually led to global cooling and the formation of sea ice [*Clark*, 1999; *Clark et al.*, 2009]. Depending on the global region, the ice sheet maxima occurred between 33.0 to 26.5 ka, while the sea level low stand took place 26.5 to 19 ka ago [*Clark et al.*, 2009]; in southwest Africa, the LGM occurred approximately 20 to 24 ka ago [*Franzese et al.*, 2006; *Clark et al.*, 2012; *Piotrowski et al.*, 2012]. The Agulhas (leakage) is largely controlled by the location of the westerly winds and the subtropical front (STF), the boundary of NADW and Southern Ocean waters [*Bard and Rickaby*, 2009; *Beal et al.*, 2011; *Caley et al.*, 2012; *Durgadoo et al.*, 2013], which were both significantly shifted to the north during the LGM. This allowed for more southern-sourced water to enter the Atlantic at the Romanche Fracture Zone *[Oppo and Fairbank, 1987; Bard and Rickab, 2009; Howe et al., 2016c]*, while the flow of NADW was significantly reduced. Therefore, the deep Atlantic's chemistry was more heavily influenced by Southern Ocean waters than it is today (Figure 12, Figure 13). The increased contribution of glacial AABW led to more radiogenic ε_{Nd} ratios in the

Cape Basin: the 'LGM' samples' ratios are $\varepsilon_{Nd(N36/6b)}$ ~-8.1±0.3 and $\varepsilon_{Nd(24/6b)}$ ~-7.7±0.3, and are significantly lower than those of glacial NADW ($\varepsilon_{Nd(GNADW)}$ ~-13.5±3.0).

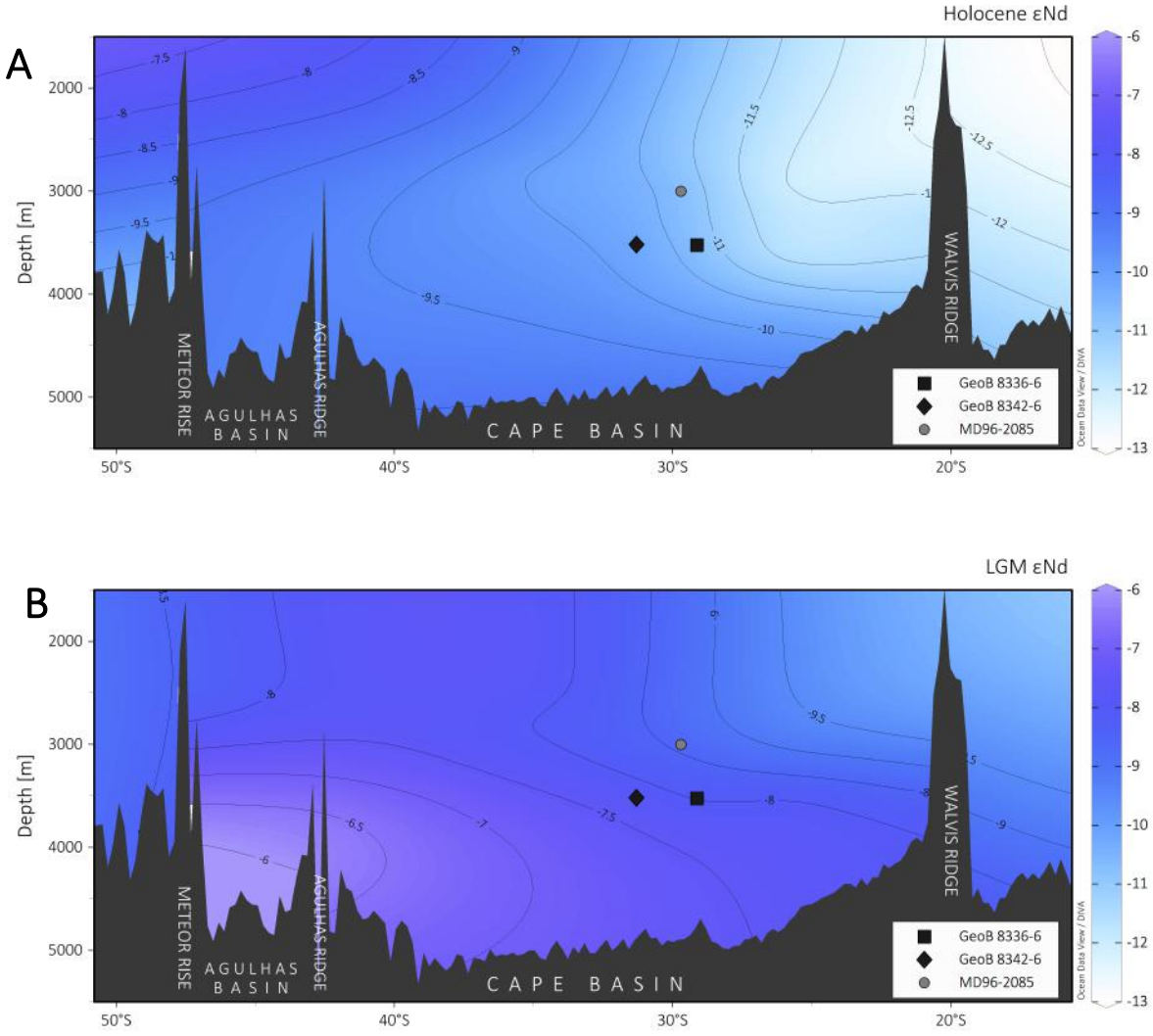

Figure 12. South to north Cross-section of the deep (>1500 m) Cape Basin showing the reconstructed (a) Holocene and (b) LGM ε_{Nd} data derived from GeoB8336-6 (''), GeoB8342-6 (''), and previous studies [*Piotrowski et al.*, 2012; *Howe et al.*, 2016c; *Wei et al.*, 2016]. As described in the text, LGM Cape Basin ε_{Nd} ratios of deep water were significantly more radiogenic. Surface and intermediate water ε_{Nd} data are not available for the Cape Basin and thus not displayed.

Maps created in ODV [*Schlitzer*, 2017].

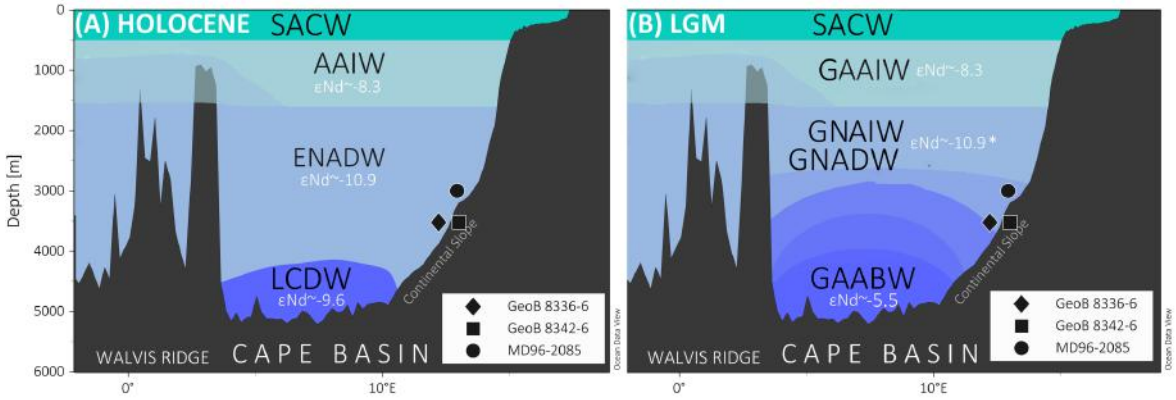

Figure 13. Cross-section along 30°S schematically showing the proposed distribution of water masses during marine isotope stages 1 (a) and 2 (b). ε_{Nd} data are taken from the references provided in the text. As noted by Howe et al. [2016c], GNADW ε_{Nd} did not vary from NADW ε_{Nd}. Therefore, ENADW ratios are expected for the Cape Basin. (cross-sections created in ODV [Schlitzer, 2017]; modelled after the processes described in the text, with ε_{Nd} data were taken from the references in the text, as well as Stichel et al. [2009].

The Agulhas leakage was reduced throughout the LGM and only regained strength with the onset of the glacial termination (Termination I), the end of the LGM [*Franzese et al.*, 2006; *Beal et al.*, 2011]. Whether AAIW flow also underwent significant changes during the LGM has been debated in the past, however, a recent study [*Howe et al.*, 2016a] found no indications for such variations in the intermediate water mass. Thus, it has been concluded that glacial AAIW (GAAIW) did not extend further into the South Atlantic [*Howe et al.*, 2016a and references therein]. Sediment studies of the Cape Basin continental slope found that the total organic carbon (TOC) was ~84% higher in comparison compared to modern levels, which suggests enhanced productivity during the LGM [*Mollenhauer et al.*, 2002]. This potential shift in productivity has been linked to the increase in upwelling and to the northward shift the Angola-Benguela front to 17°S during the LGM and MIS3 [*Jansen et al.*, 1996; *Little et al.*, 1997; *Pichevin et al.*, 2005].

The last glacial termination started around ~19 ka and lasted until the early Holocene (~11 ka) [*Denton et al.*, 2010; *Clark et al.*, 2012]. The rise of global temperatures induced the melting of the ice sheets, which led to an average global sea level increase of approximately 80 m. Approximately 17.5 thousand years ago, the CO_2 concentrations rose [*Clark et al.*, 2012] by ~80 ppm [*Roberts et al.*, 2016]. The release of freshwater caused variations in the buoyancy-driven ocean circulation in the South Atlantic. During the LGM, the sea ice acted as a barrier between the deep water masses, and

thus the deep water-to-surface ventilation was significantly impacted. However, as the ice sheets started to melt, this exchange was reestablished [*Roberts et al.*, 2016]. Since the Agulhas leakage is known to play an important role in the (modern) MOC, it has been hypothesized that the sudden increase in subtropical water export into the Atlantic during the glacial termination accelerated the rate at which Earth entered the next episode of interglacial climate [*Beal et al.*, 2011 and references therein]. Warming continued and the influence of northern-sourced water on the Cape Basin water masses grew (Figure 12, Figure 13) [*Roberts et al.*, 2016]. Approximately 9 to 8 ka ago, the Cape Basin entered the Holocene Climatic Optimum [*Gingele*, 1996]. The study of the 'Holocene' samples suggests that Cape Basin Holocene circulation was essentially the same as reported today ($\varepsilon_{Nd(N36/6a)}$ = -10.7±0.3 & $\varepsilon_{Nd(N42/6a\ mean)}$ = -10.20±0.40; modern ENADW (-10.9±1.2), and thus provides further evidence for the reduced influence of southern-sourced water masses in comparison to the LGM. Therefore, these findings suggest that the regional water mass dynamics did not change substantially over the last 5 to 9 thousand years.

5.4.2 IMPLICATIONS FOR TERMINATION I DERIVED FROM MIS3

In comparison to the LGM, only a few studies [e.g. *Rutberg et al.*, 2000; *Piotrowski et al.*, 2005] have been carried out that assess the MIS3 water mass variations in the Cape Basin. The more radiogenic ε_{Nd} ratios of the MIS3 samples, in comparison the Holocene and modern ε_{Nd} ratios, indicate that the Cape Basin deep waters were more heavily influenced by southern water masses during MIS3. These observations support those reported for the last glacial termination [*Rutberg et al.*, 2000; *Piotrowski et al.*, 2005], and allow for the speculation that the AMOC underwent changes during Termination I that resemble the oceanographic setting of MIS3. However, while the water mass reconstruction suggests a similar setup, it is important to note that MIS3 was an interglacial, thus MIS3 took much longer to develop and remained in this state for a longer time. Termination I, on the other hand, marks the transition from a cold to warm period and evolved at a much quicker rate. Nonetheless, further examining MIS3 remains important for a better understanding of the evolution of today's climate and ocean system: it is now believed that the extent of deglaciation during MIS3 was essential for the

Holocene becoming an interstadial [*Tzedakis et al.*, 2017]. Therefore, further studying the ocean circulation of MIS3 could provide valuable information not only on the climate of the past but also for future climate models.

6 CONCLUSION

Sediment cores GeoB8336-6 and GeoB8342-6 were dated based on their sediment reflectance profiles in correlation to other cores in the region, and the core sample intervals of the Holocene, LGM and MIS3 were defined. Mixed planktic and bulk foraminifera samples from these three depth intervals were taken and analyzed for their Nd isotope systematics following the sample preparation protocol proposed by the Cambridge group. This procedure proved to be a reliable method to prepare both mixed planktic and bulk foraminifera tests and is therefore recommended for further ε_{Nd} studies of (planktic) foraminifera at UCT. The Nd isotope systematics of all samples exhibit no signs of detrital or pore water contamination, and were found to be in good agreement with those reported in the literature. Therefore, the foraminifera analyzed in this study proved to be a reliable proxy for ambient bottom water. Further, the mixed planktic foraminifera samples and non-selective bulk foraminifera samples taken at the same depth intervals show the same ε_{Nd} ratios within error. This suggests that in-place bulk foraminifera samples may be used as a tool for reconstructing ambient bottom water ε_{Nd} ratios. However, more research should be conducted to further support these findings.

Atmospherical and oceanographic shifts during the LGM led to a reduced export of NADW into the Cape Basin, which allowed for Antarctic-sourced waters to intrude further northward. The ε_{Nd} ratios of the 'LGM' samples were the most radiogenic ratios measured in this study ($\varepsilon_{Nd(N36/6b)}$ = -8.1±0.3 and $\varepsilon_{Nd(N42/6b)}$ = -7.7±0.3), which can be attributed to the greater importance of southern waters during the LGM and thus reflect the change in the extent of glacial AABW in comparison to the modern AABW. 'Holocene' samples exhibit ε_{Nd} ratios of -10.7±0.3 (N36/6a) and -10.20±0.40 (N42/6a mean),

which lie within the range of those reported for the modern ENADW. This provides further proof that the northern-sourced NADW is the main contributor to Holocene deep waters of the Cape Basin and that the water masses ~30°S did not vary significantly since the Holocene Climatic Optimum. The samples of the interglacial stage preceding the LGM show ratios that lie in between those observed in the LGM and Holocene. The maximum of MIS3 was notably cooler than the Holocene optimum, and it is hypothesized that the ocean circulation during MIS3 was similar to that at Termination I.

7 LIMITATIONS AND FUTURE RESEARCH

Overall, all objectives of this study were met: ε_{Nd} ratios were successfully measured and proved to be reliable proxies for LGM and Holocene seawater. The ε_{Nd} ratios of this study therefore further extend the 'Nd database' of the Late Quaternary southeastern Atlantic. The sample preparation procedure presented in this study was found to be reliable for the removal of terrigenous sediment and is thus recommended for further foraminiferal ε_{Nd} studies. However, owing to time constraints, the cores were only dated based on their L* profile and correlation to the other cores. Further studies using oxygen stable isotope dating are to be conducted in the future to enhance age models for the cores (study by Eugene Bergh). In addition to obtaining the ε_{Nd} ratios of planktic and bulk foraminifera, one of the initial aims of this study was to measure the ε_{Nd} ratios of benthic foraminifera. However, due to the low abundance of benthic foraminifera in the sediment core samples (commonly <2 mg per sample), the Nd isotope analysis could not be conducted. As previously suggested, benthic foraminifera and planktic foraminifera commonly exhibit the same ε_{Nd} ratios, therefore no deviation of the ε_{Nd} ratios of benthic foraminifera from the measured ε_{Nd} from bulk and planktic foraminifera is expected. Finally, the bulk and planktic foraminifera studied exhibit the same ε_{Nd} ratios, which suggests that bulk foraminifera could be used for ε_{Nd} studies in the future. Further research needs to be conducted to further test this hypothesis.

ACKNOWLEDGEMENT

First and foremost, I would like to express my sincere gratitude to my supervisor, Assoc. Prof. John Compton for his valuable advice, continuous support and guidance throughout the process of writing this thesis.

A very special thanks also to Eugene Bergh for his help with identifying the foraminifera species and core depths. I wish to thank everyone who helped process and analyze my samples, particularly Christel Tinguely (UCT Quadrupole ICP-MS facility), Fayrooza Rawoot (UCT MC-ICP-MS Facility) and Petrus le Roux (UCT MC-ICP-MS Facility).

Finally, I would like to thank my parents and my brother Leon for their tremendous love and support, and for giving me the opportunity to study at the University of Cape Town. I am eternally grateful for your encouragement and all the amazing opportunities you have given me.

[This page intentionally left blank]

BIBLIOGRAPHY

Bard, E., and R. E. M. Rickaby (2009), Migration of the subtropical front as a modulator of glacial climate., *Nature*, *460*(7253), 380–3, doi:10.1038/nature08189.

Bau, M., and P. Dulski (1995), Comparative study of yttrium and rare-earth element behaviours in fluorine-rich hydrothermal fluids, *Contrib. to Mineral. Petrol.*, *119*(2–3), 213–223, doi:10.1007/BF00307282.

Bau, M., and P. Dulski (1996), Distribution of yttrium and rare-earth elements in the Penge and Kuruman iron-formations, Transvaal Supergroup, South Africa, *Precambrian Res.*, *79*(79), 37–55, doi:10.1016/0301-9268(95)00087-9.

Bau, M., A. Koschinsky, P. Dulski, and J. R. Hein (1996), Comparison of the partitioning behaviours of yttrium, rare earth elements, and titanium between hydrogenetic marine ferromanganese crusts and seawater, *Geochim. Cosmochim. Acta*, *60*(10), 1709–1725, doi:10.1016/0016-7037(96)00063-4.

Beal, L. M., W. P. M. De Ruijter, A. Biastoch, and R. Zahn (2011), On the role of the Agulhas system in ocean circulation and climate., *Nature*, *472*(7344), 429–36, doi:10.1038/nature09983.

Berger, A., J. Imbrie, J. Hays, G. Kukla, and B. Saltzman (1984), *Milankovitch and climate: understanding the response to astronomical forcing. Proceedings of the NATO Advanced Research Workshop, Palisades, 1982. Two volumes.*

von Blankenburg, F. (1999), Tracing Past Ocean Circulation?, *Science (80-.).*, *286*(5446), 1862–1863, doi:10.1126/science.286.5446.1862b.

Bolhar, R., B. S. Kamber, S. Moorbath, C. M. Fedo, and M. J. Whitehouse (2004), Characterisation of early Archaean chemical sediments by trace element signatures, *Earth Planet. Sci. Lett.*, *222*(1), 43–60, doi:10.1016/j.epsl.2004.02.016.

Boyle, E. A., and L. Keigwin (1987), North Atlantic thermohaline circulation during the past 20,000 years linked to high-latitude surface temperature, *Nature*, *330*, 35–40, doi:10.1038/330035a0.

Boyle, E. A., and L. D. Keigwin (1982), Deep Circulation of the North Atlantic over the Last 200,000 Years: Geochemical Evidence, *Science (80-.).*, *218*(4574), 784–787, doi:10.1126/science.218.4574.784.

Broecker, W. S. (1982), Ocean chemistry during glacial time, *Geochim. Cosmochim. Acta*, *46*(10), 1689–1705, doi:10.1016/0016-7037(82)90110-7.

Broecker, W. S., and G. H. Denton (1990), The role of ocean-atmosphere reorganizations in glacial cycles, *Quat. Sci. Rev.*, *9*(4), 305–341, doi:10.1016/0277-3791(90)90026-7.

Brühl, R. (2015), Abscissa for Mac,

Burton, K. W., and D. Vance (2000), Glacial-interglacial variations in the neodymium isotope composition of seawater in the Bay of Bengal recorded by planktonic foraminifera, *Earth Planet. Sci. Lett.*, *176*(3–4), 425–441, doi:10.1016/S0012-821X(00)00011-X.

Caley, T., J. Giraudeau, B. Malaizé, L. Rossignol, and C. Pierre (2012), Agulhas leakage as a key process in the modes of Quaternary climate changes., *Proc. Natl. Acad. Sci. U. S. A.*, *109*(18), 6835–9, doi:10.1073/pnas.1115545109.

Chen, M. Te, Y.-P. Chang, C.-C. Chang, L. Wang, W. Chung-Ho;, and E.-F. Yu (2002a), (Table 1) Age control points of sediment core MD96-2085., , doi:doi:10.1594/PANGAEA.736656.

Chen, M. Te, Y. P. Chang, C. C. Chang, L. W. Wang, C. H. Wang, and E. F. Yu (2002b), Late Quaternary sea-surface temperature variations in the southeast Atlantic: A planktic foraminifer faunal record of the past 600 000 yr (IMAGES II MD962085), *Mar. Geol.*, *180*(1–4), 163–181, doi:10.1016/S0025-3227(01)00212-2.

Clark, P. U. (1999), Northern Hemisphere Ice-Sheet Influences on Global Climate Change, *Science (80-.).*, *286*(5442), 1104–1111, doi:10.1126/science.286.5442.1104.

Clark, P. U., N. G. Pisias, T. F. Stocker, and A. J. Weaver (2002), The role of the thermohaline circulation in abrupt climate change, *Nature*, *415*(6874), 863–869, doi:10.1038/415863a.

Clark, P. U. et al. (2009), The Last Glacial Maximum., *Science*, *325*(5941), 710–4, doi:10.1126/science.1172873.

Clark, P. U. et al. (2012), Global climate evolution during the last deglaciation, *Proc. Natl. Acad. Sci. U. S. A.*, *109*(19), 1134–1142, doi:10.1073/pnas.1116619109/-/DCSupplemental.www.pnas.org/cgi/doi/10.1073/pnas.1116619109.

Claude, C., and B. Hamelin (2007), Chapter Fifteen Isotopic Tracers of Water Masses and Deep Currents, *Dev. Mar. Geol.*, *1*, 645–679, doi:10.1016/S1572-5480(07)01020-2.

Compton, J. S., and J. G. Wiltshire (2009), Terrigenous sediment export from the western margin of South Africa on glacial to interglacial cycles, *Mar. Geol.*, *266*(1–4), 212–222, doi:10.1016/j.margeo.2009.08.013.

Compton, J. S., C. T. Herbert, M. T. Hoffman, R. R. Schneider, and J.-B. Stuut (2010), A tenfold increase in the Orange River mean Holocene mud flux: implications for soil erosion in South Africa, *The Holocene*, *20*(1), 115–122, doi:10.1177/0959683609348860.

Cruse, A. M., T. W. Lyons, and D. L. Kidder (2000), Rare-earth element behavior in phosphates and organic-rich host shales: an example from the Upper Carboniferous of midcontinent North America, *SEPM Spec. Publ.*, *66*, 445–453, doi:10.2110/pec.00.66.0445.

Curry, W. B., and G. P. Lohmann (1982), Carbon isotopic changes in benthic foraminifera from the western South Atlantic: Reconstruction of glacial abyssal circulation patterns, *Quat. Res.*, *18*(2), 218–235, doi:10.1016/0033-5894(82)90071-0.

Curry, W. B., and D. W. Oppo (2005), Glacial water mass geometry and the distribution of delta C-13 of Sigma CO2 in the western Atlantic Ocean *, *Paleoceanography*, *20*, 1017 2004PA001021, doi:doi:10.1029/2004PA001021.

Delworth, T. L., P. U. Clark, M. Holland, W. E. Johns, T. Kuhlbrodt, J. Lynch-Stieglitz, C. Morrill, R. Seager, A. J. Weaver, and R. Zhang (2008), The Potential for Abrupt Change in the Atlantic Meridional Overturning Circulation, *Abrupt Clim. Chang.*, 258–359.

Denoyelle, M., F. J. Jorissen, D. Martin, F. Galgani, and J. Miné (2010), Comparison of benthic foraminifera and macrofaunal indicators of the impact of oil-based drill mud disposal, *Mar. Pollut. Bull.*, *60*(11), 2007–2021, doi:10.1016/j.marpolbul.2010.07.024.

Denton, G. H., R. F. Anderson, J. R. Toggweiler, R. L. Edwards, J. M. Schaefer, and A. E. Putnam (2010), The Last Glacial Termination, *Science (80-.).*, *328*(June), 1652–1656, doi:10.1126/science.1184119.

Diekmann, B., and G. Kuhn (2002), Sedimentary record of the mid-Pleistocene climate transition in the southeastern South Atlantic (ODP Site 1090), *Palaeogeogr. Palaeoclimatol. Palaeoecol.*, *182*(3–4), 241–258, doi:10.1016/S0031-0182(01)00498-9.

Dingle, R. V. et al. (1987), Deep-sea sedimentary environments around southern Africa (south-east Atlantic and south-west Indian oceans, *Ann. South African museum*, *98*(1).

Duncombe Rae, C. (1991), Agulhas retroflection rings in the South Atlantic Ocean: an overview, *South African J. Mar. Sci.*, *11*, 327–344, doi:10.2989/025776191784287574.

Duplessy, J. C., N. J. Shackleton, R. G. Fairbanks, L. Labeyrie, D. Oppo, and N. Kallel (1988), Deepwater source variations during the last climatic cycle and their impact on the global deepwater circulation, *Paleoceanography*, *3*(3), 343–360, doi:10.1029/PA003i003p00343.

Durgadoo, J. V., B. R. Loveday, C. J. C. Reason, P. Penven, A. Biastoch, J. V. Durgadoo, B. R. Loveday, C. J. C. Reason, P. Penven, and A. Biastoch (2013), Agulhas Leakage Predominantly Responds to the Southern Hemisphere Westerlies, *J. Phys. Oceanogr.*, *43*(10), 2113–2131, doi:10.1175/JPO-D-13-047.1.

Eagles, G. (2007), New angles on South Atlantic opening, *Geophys. J. Int.*, *168*(1), 353–361, doi:10.1111/j.1365-246X.2006.03206.x.

Elderfield, H., and M. J. Greaves (1982), The rare earth elements in seawater, *Nature*, doi:10.1038/296214a0.

Elderfield, H., P. Ferretti, M. Greaves, S. J. Crowhurst, I. N. McCave, D. a Hodell, and A. M. Piotrowski (2012), Evolution of Ocean Temperature and Ice Volume Through the Mid-Pleistocene Climate Transition, *Science (80-.).*, *337*(August), 704–709, doi:10.1594/PANGAEA.786205.

Elmore, A. C., A. M. Piotrowski, J. D. Wright, and A. E. Scrivner (2011), Testing the extraction of past seawater Nd isotopic composition from North Atlantic deep sea sediments and foraminifera, *Geochemistry, Geophys. Geosystems*, *12*(9), doi:10.1029/2011GC003741.

Emery, W. J., Meincke, J. (1986), Global water masses: summary and review, *Oceanol. Acta*, *9*(4), 383–391.

Emery, K. O., E. Uchupi, C. O. Bowin, J. Phillips, and E. S. W. Simpson (1975), Continental margin off Western Africa; Cape Saint Francis (South Africa) to Walvis Ridge (South-West Africa), *Am. Assoc. Pet. Geol. Bull.*, *59*(1), 3–59.

Franzese, A. M., S. R. Hemming, S. L. Goldstein, and R. F. Anderson (2006), Reduced Agulhas Leakage during the Last Glacial Maximum inferred from an integrated provenance and flux study, *Earth Planet. Sci. Lett.*, *250*(1–2), 72–88, doi:10.1016/j.epsl.2006.07.002.

Gebbie, G. (2014), How much did Glacial North Atlantic Water shoal?, *Paleoceanography*, *29*(3), 190–209, doi:10.1002/2013PA002557.

Gingele, F. X. (1996), Holocene climatic optimum in southwest Africa - Evidence from the marine clay mineral record, *Palaeogeogr. Palaeoclimatol. Palaeoecol.*, *122*, 77–87, doi:10.1016/0031-0182(96)00076-4.

Goldstein, S. L., and S. R. Hemming (2013), Long-lived Isotopic Tracers in Oceanography, Paleoceanography, and Ice-sheet Dynamics, in *Treatise on Geochemistry: Second Edition*, vol. 8, pp. 453–483.

Gordon, A. L., R. F. Weiss, W. M. Smethie, and M. J. Warner (1992), Thermocline and intermediate water communication between the South Atlantic and Indian Oceans, *J. Geophys. Res.*, *97*(C5), 7223, doi:10.1029/92JC00485.

Grousset, F. E., P. E. Biscaye, A. Zindler, J. Prospero, and R. Chester (1988), Neodymium isotopes as tracers in marine sediments and aerosols: North Atlantic, *Earth Planet. Sci. Lett.*, *87*(4), 367–378, doi:10.1016/0012-821X(88)90001-5.

Gutjahr, M., M. Frank, C. H. Stirling, V. Klemm, T. van de Flierdt, and A. N. Halliday (2007), Reliable extraction of a deepwater trace metal isotope signal from Fe-Mn oxyhydroxide coatings of marine sediments, *Chem. Geol.*, *242*(3–4), 351–370, doi:10.1016/j.chemgeo.2007.03.021.

Hemming, S. (2004), Heinrich events: Massive late Pleistocene detritus layers of the North Atlantic and their global climate imprint, *Rev. Geophys.*, *42*, 1–43, doi:10.1029/2003RG000128.1.INTRODUCTION.

Herbert, C. T., and J. S. Compton (2007), Geochronology of Holocene sediments on the western margin of South Africa, *South African J. Geol.*, *110*(2–3), 327–338, doi:10.2113/gssajg.110.2-3.327.

Howe, J. N. W., A. M. Piotrowski, D. W. Oppo, K.-F. Huang, S. Mulitza, C. M. Chiessi, and J. Blusztajn (2016a), Antarctic Intermediate Water circulation in the South Atlantic over the past 25,000 years, *Paleoceanography*, *31*(10), 1302–1314, doi:10.1002/2016PA002975.

Howe, J. N. W., A. M. Piotrowski, T. L. Noble, S. Mulitza, C. M. Chiessi, and G. Bayon (2016b), *Holocene and Last Glacial Maximum Atlantic neodymium isotopes. Supplement to: Howe, JNW et al. (2016): North Atlantic Deep Water Production during the Last Glacial Maximum. Nature Communications, 7, 11765, doi:10.1038/ncomms11765*.

Howe, J. N. W., A. M. Piotrowski, T. L. Noble, S. Mulitza, C. M. Chiessi, and G. Bayon (2016c), North Atlantic Deep Water Production during the Last Glacial Maximum, *Nat. Commun.*, *7*, 11765, doi:10.1038/ncomms11765.

Imbrie, J. et al. (1992), On the Structure and Origin of Major Glaciation Cycles 1. Linear Responses to Milankovitch Forcing, *Paleoceanography*, *7*(6), 701–738, doi:10.1029/92PA02253.

Jacobsen, S. B., and G. J. Wasserburg (1980), Sm-Nd isotopic evolution of chondrites, *Earth Planet. Sci. Lett.*, *50*(1), 139–155, doi:10.1016/0012-821X(80)90125-9.

Jansen, J. H. F., E. Ufkes, and R. R. Schneider (1996), Late Quaternary movements of the Angola-Benguela Front, SE Atlantic, and implications for advection in the equatorial ocean, in *The South Atlantic: Present and past circulation*, pp. 553–575.

Jeandel, C. (1993), Concentration and isotopic composition of Nd in the South Atlantic Ocean, *Earth Planet. Sci. Lett.*, *117*(3–4), 581–591, doi:10.1016/0012-821X(93)90104-H.

Kerr, R. A. (2005), Paleoclimate: Ocean flow amplified, not triggered, climate change, *Science (80-.).*, *307*(5717), 1854, doi:10.1126/science.307.5717.1854a.

Kimoto, K. (2015), Planktic Foraminifera, in *Marine Protists*, pp. 129–178.

Kraft, S., M. Frank, E. C. Hathorne, and S. Weldeab (2013), Assessment of seawater Nd isotope signatures extracted from foraminiferal shells and authigenic phases of Gulf of Guinea sediments, *Geochim. Cosmochim. Acta*, *121*, 414–435, doi:10.1016/j.gca.2013.07.029.

Kucera, M. (2007), Chapter Six Planktonic Foraminifera as Tracers of Past Oceanic Environments, pp. 213–262.

Li, Y. H., and J. E. Schoonmaker (2013), Chemical Composition and Mineralogy of Marine Sediments, in *Treatise on Geochemistry: Second Edition*, vol. 9, pp. 1–32.

van der Lingen, C. D., L. J. Shannon, P. Cury, A. Kreiner, C. L. Moloney, J.-P. Roux, and F. Vaz-Velho (2006), Benguela - Predicting a Large Marine Ecosystem, *Large Mar. Ecosyst.*, *14*, 147–184, doi:10.1016/S1570-0461(06)80013-3.

Lisiecki, L. E., and M. E. Raymo (2005), A Plio-Pleistocene stack of 57 globally distributed benthic [delta]18O records, *Paleoceanography*, *20*, PA1003, doi:10.1029/2004PA001071.

Little, M. G., R. R. Schneider, D. Kroon, B. Price, T. Bickert, and G. Wefer (1997), Rapid palaeoceanographic changes in the Benguela Upwelling System for the last 160,000 years as indicated by abundances of planktonic foraminifera, *Palaeogeogr. Palaeoclimatol. Palaeoecol.*, *130*(1–4), 135–161, doi:10.1016/S0031-0182(96)00136-8.

Lumpkin, R., and K. Speer (2007), Global Ocean Meridional Overturning, *J. Phys. Oceanogr.*, *37*(10), 2550–2562, doi:10.1175/JPO3130.1.

Lutjeharms, J. R., F. a Shillington, and C. M. Rae (1991), Observations of extreme upwelling filaments in the southeast atlantic ocean., *Science*, *253*(5021), 774–776, doi:10.1126/science.253.5021.774.

Lutjeharms, J. R. E. (2006), *The Agulhas Current*.

Lutjeharms, J. R. E., and I. J. Ansorge (2001), The Agulhas Return Current, *J. Mar. Syst.*, *30*(1–2), 115–138, doi:10.1016/S0924-7963(01)00041-0.

Lutjeharms, J. R. E., and R. C. van Ballegooyen (1988), The Retroflection of the Agulhas Current, *J. Phys. Oceanogr.*, *18*(11), 1570–1583, doi:10.1175/1520-0485(1988)018<1570:TROTAC>2.0.CO;2.

Lutjeharms, J. R. E., and J. M. Meeuwis (1987), The extent and variability of South-East Atlantic upwelling, *South African J. Mar. Sci.*, *5*(1), 51–62, doi:10.2989/025776187784522621.

Lutjeharms, J. R. E., and P. L. Stockton (1987), Kinematics of the upwelling front off southern Africa, *South African J. Mar. Sci.*, *5*(1), 35–49, doi:10.2989/025776187784522612.

Lynch-Stieglitz, J., and T. M. Marchitto (2013), Tracers of Past Ocean Circulation, in *Treatise on Geochemistry: Second Edition*, vol. 8, pp. 435–452.

Lynch-Stieglitz, J. et al. (2007), Atlantic meridional overturning circulation during the Last Glacial Maximum., *Science*, *316*(5821), 66–69, doi:10.1126/science.1137127.

Marchal, O., and W. B. Curry (2008), On the Abyssal Circulation in the Glacial Atlantic, *J. Phys. Oceanogr.*, *38*, 2014–2037, doi:10.1175/2008JPO3895.1.

Martin, E. E., S. W. Blair, G. D. Kamenov, H. D. Scher, E. Bourbon, C. Basak, and D. N. Newkirk (2010), Extraction of Nd isotopes from bulk deep sea sediments for paleoceanographic studies on Cenozoic time scales, *Chem. Geol.*, *269*(3–4), 414–431, doi:10.1016/j.chemgeo.2009.10.016.

Van Meerbeeck, C. J., H. Renssen, and D. M. Roche (2008), How did Marine Isotope Stage 3 and Last Glacial Maximum climates differ? Perspectives from equilibrium simulations, *Clim. Past Discuss.*, *4*(5), 1115–1158, doi:10.5194/cpd-4-1115-2008.

Míková, J., and P. Denková (2007), Modified chromatographic separation scheme for Sr and Nd isotope analysis in geological silicate samples, *J. Geosci.*, *52*(3–4), 221–226, doi:10.3190/jgeosci.015.

Mollenhauer, G., R. R. Schneider, P. J. Müller, V. Spieß, and G. Wefer (2002), Glacial/interglacial variablity in the Benguela upwelling system: Spatial distribution and budgets of organic carbon accumulation, *Global Biogeochem. Cycles*, *16*(4), 81-1-81–15, doi:10.1029/2001GB001488.

Murray, J. W. (2006), *Ecology and Applications of Benthic Foraminifera*.

Nelson, G., and L. Hutchings (1983), The Benguela upwelling area, *Prog. Oceanogr.*, *12*(3), 333–356, doi:10.1016/0079-6611(83)90013-7.

Neuendorf, K. K. E. (2005), *Glossary of Geology*, 5th ed., edited by J. A. Jackson, J. P. Mehl, and K. K. E. Neuendorf, Springer Science & Business Media, 2005, Alexandria, Virginia.

Nürnberg, D., and R. D. Müller (1991), The tectonic evolution of the South Atlantic from Late Jurassic to present, *Tectonophysics*, *191*(1–2), 27–53, doi:10.1016/0040-1951(91)90231-G.

Oppo, D. W., and R. G. Fairbanks (1987), Variability in the deep and intermediate water circulation of the Atlantic Ocean during the past 25,000 years: Northern Hemisphere modulation of the Southern Ocean, *Earth Planet. Sci. Lett.*, *86*(1), 1–15, doi:10.1016/0012-821X(87)90183-X.

Palmer, M. R. (1985), Rare earth elements in foraminifera tests, *Earth Planet. Sci. Lett.*, *73*(2–4), 285–298, doi:10.1016/0012-821X(85)90077-9.

Palmer, M. R., and H. Elderfield (1985), Variations in the Nd isotopic composition of foraminifera from Atlantic Ocean sediments, *Earth Planet. Sci. Lett.*, *73*(2–4), 299–305, doi:10.1016/0012-821X(85)90078-0.

Peterson, R. G., and L. Stramma (1991), Upper-level circulation in the South Atlantic Ocean, *Prog. Oceanogr.*, *26*(1), 1–73, doi:10.1016/0079-6611(91)90006-8.

Pichevin, L., M. Cremer, J. Giraudeau, and P. Bertrand (2005), A 190 ky record of lithogenic grain-size on the Namibian slope: Forging a tight link between past wind-strength and coastal upwelling dynamics, *Mar. Geol.*, *218*(1–4), 81–96, doi:10.1016/j.margeo.2005.04.003.

Piepgras, D. J., and G. J. Wasserburg (1980), Neodymium isotopic variations in seawater, *Earth Planet. Sci. Lett.*, *50*(1), 128–138, doi:10.1016/0012-821X(80)90124-7.

Piepgras, D. J., G. J. Wasserburg, and E. J. Dasch (1979), The isotopic composition of Nd in different ocean masses, *Earth Planet. Sci. Lett.*, *45*(2), 223–236, doi:10.1016/0012-821X(79)90125-0.

Pin, C., and J. F. Santos Zalduegui (1997), Sequential separation of light rare-earth elements, thorium and uranium by miniaturized extraction chromatography: Application to isotopic analyses of silicate rocks, *Anal. Chim. Acta*, *339*(1–2), 79–89, doi:10.1016/S0003-2670(96)00499-0.

Pin, C., D. Briot, C. Bassin, and F. Poitrasson (1994), Concomitant separation of strontium and samarium-neodymium for isotopic analysis in silicate samples, based on specific extraction chromatography, *Anal. Chim. Acta*, *298*(2), 209–217, doi:10.1016/0003-2670(94)00274-6.

Piotrowski, A. M., S. L. Goldstein, S. R. Hemming, R. G. Fairbanks, and D. R. Zylberberg (2008), Oscillating glacial northern and southern deep water formation from combined neodymium and carbon isotopes, *Earth Planet. Sci. Lett.*, *272*(1–2), 394–405, doi:10.1016/j.epsl.2008.05.011.

Piotrowski, A. M., A. Galy, J. A. L. Nicholl, N. Roberts, D. J. Wilson, J. A. Clegg, and J. Yu (2012), Reconstructing deglacial North and South Atlantic deep water sourcing using foraminiferal Nd isotopes, *Earth Planet. Sci. Lett.*, *357–358*, 289–297, doi:10.1016/j.epsl.2012.09.036.

Piotrowski, A. M. A., S. S. L. Goldstein, S. R. Hemming, and R. G. Fairbanks (2005), Temporal relationships of carbon cycling and ocean circulation at glacial boundaries, *Science (80-.).*, *307*(March), 1933–1938, doi:10.1126/science.1104883.

Rabinowitz, P. D. (1976), Geophysical study of the continental margin of southern Africa, *Geol. Soc. Am. Bull.*, *87*(11), 1643 LP-1653.

Rau, A. J., J. Rogers, J. R. E. Lutjeharms, J. Giraudeau, J. A. Lee-Thorp, M. T. Chen, and C. Waelbroeck (2002), A 450-kyr record of hydrological conditions on the western Agulhas Bank Slope, south of Africa, *Mar. Geol.*, *180*(1–4), 183–201, doi:10.1016/S0025-3227(01)00213-4.

Richardson, S. H., A. J. Erlank, A. R. Duncan, and D. L. Reid (1982), Correlated Nd, Sr and Pb isotope variation in Walvis Ridge basalts and implications for the evolution of their mantle source, *Earth Planet. Sci. Lett.*, *59*(2), 327–342, doi:10.1016/0012-821X(82)90135-2.

Rickli, J., M. Frank, and A. N. Halliday (2009), The hafnium-neodymium isotopic composition of Atlantic seawater, *Earth Planet. Sci. Lett.*, *280*(1–4), 118–127, doi:10.1016/j.epsl.2009.01.026.

Roberts, J., J. Gottschalk, L. C. Skinner, V. L. Peck, S. Kender, H. Elderfield, C. Waelbroeck, N. Vázquez Riveiros, and D. A. Hodell (2016), Evolution of South Atlantic density and chemical stratification across the last deglaciation., *Proc. Natl. Acad. Sci. U. S. A.*, 1511252113-, doi:10.1073/pnas.1511252113.

Roberts, N. L., A. M. Piotrowski, J. F. McManus, and L. D. Keigwin (2010), Synchronous deglacial overturning and water mass source changes., *Science (80-.).*, *327*(2009), 75–78, doi:10.1126/science.1178068.

Roberts, N. L., A. M. Piotrowski, H. Elderfield, T. I. Eglinton, and M. W. Lomas (2012), Rare earth element association with foraminifera, *Geochim. Cosmochim. Acta*, *94*, 57–71, doi:10.1016/j.gca.2012.07.009.

de Ruijter, W. P. M., A. Biastoch, S. S. Drijfhout, J. R. E. Lutjeharms, R. P. Matano, T. Pichevin, P. J. van Leeuwen, and W. Weijer (1999), Indian-Atlantic interocean exchange: Dynamics, estimation and impact, *J. Geophys. Res.*, *104*(C9), 20885, doi:10.1029/1998JC900099.

Rutberg, R. L., S. R. Hemming, and S. L. Goldstein (2000), Reduced North Atlantic Deep Water flux to the glacial Southern Ocean inferred from neodymium isotope ratios, *Nature*, *405*, 935–938, doi:10.1038/35016049.

Sachs, J. P., R. F. Anderson, and S. J. Lehman (2001), Glacial surface temperatures of the southeast Atlantic Ocean., *Science*, *293*(5537), 2077–2079, doi:10.1126/science.1063584.

Sarmiento, J. L., J. Dunne, A. Gnanadesikan, R. M. Key, K. Matsumoto, and R. Slater (2002), A new estimate of the CaCO3 to organic carbon export ratio, *Global Biogeochem. Cycles*, *16*(4), 1107, doi:10.1029/2002GB001919.

Schlitzer, R. (2017), Ocean Data View,

Schmiedl, G., A. Mackensen, and P. J. Müller (1997), Recent benthic foraminifera from the eastern South Atlantic Ocean: Dependence on food supply and water masses, *Mar. Micropaleontol.*, *32*(3–4), 249–287, doi:10.1016/S0377-8398(97)00023-6.

Schmittner, A., J. C. H. Chiang, and S. R. Hemming (2007), Introduction: The Ocean's Meridional Overturning Circulation, in *Ocean Circulation: Mechnisms and Impacts*, vol. 173, edited by A. Schmittner, J. C. H. Chiang, and S. R. Hemming, American Geophysical Union.

Schmittner, A., J. C. H. Chiang, and S. R. Hemming (2013), Introduction: The Ocean's Meridional Overturning Circulation, *Ocean Circ. Mech. Impacts - Past Futur. Chang. Merid. Overturning*, 1–4, doi:10.1029/173GM02.

Schneider, R. et al. (2003), *Report and Preliminary Results of Meteor Cruise M 57/1, Cape Town - Walvis Bay, 20.01 - 08.02.2003*, Bremen.

Schneider, R. R. (2003a), *Color data of sediment core GeoB8336-6*.

Schneider, R. R. (2003b), *Color data of sediment core GeoB8342-6*.

Scrutton, R. A. (1976), Crustal Structure at the Continental Margin South of South Africa, *Geophys. J. Astron. Soc.*, *44*, 601–623.

van Sebille, E., W. E. Johns, and L. M. Beal (2012), Does the vorticity flux from Agulhas rings control the zonal pathway of NADW across the South Atlantic?, *J. Geophys. Res. Ocean.*, *117*(5), doi:10.1029/2011JC007684.

Shannon, L. V, and G. Nelson (1996), The Benguela: Large Scale Features and Processes and System Variability, in *The South Atlantic: Present and Past Circulation*, pp. 163–210, Springer Berlin Heidelberg, Berlin, Heidelberg.

Shillington, F. A. (1998), The Benguela Upwelling System off Southwestern Africa, *Sea, vol 11. Ed. by A.R. Robinson K.H. Brink*, *11*, 583–604.

Stichel, T., M. Frank, J. Rickli, and B. A. Haley (2012), The hafnium and neodymium isotope composition of seawater in the Atlantic sector of the Southern Ocean, *Earth Planet. Sci. Lett.*, *317–318*, 282–294, doi:10.1016/j.epsl.2011.11.025.

Stramma, L., and M. England (1999), On the water masses and mean circulation of the South Atlantic Ocean, *J. Geophys. Res.*, *104*(C9), 20863–20883, doi:10.1029/1999JC900139.

Sverdrup, H., M. Johnson, and R. Fleming (1942), The Oceans: Their Physics, Chemistry and General Biology, *Oceanography*, 1104, doi:10.2307/210609.

Tachikawa, K., C. Jeandel, and M. Roy-Barman (1999), A new approach to the Nd residence time in the ocean: The role of atmospheric inputs, *Earth Planet. Sci. Lett.*, *170*(4), 433–446, doi:10.1016/S0012-821X(99)00127-2.

Tachikawa, K., A. M. Piotrowski, and G. Bayon (2014), Neodymium associated with foraminiferal carbonate as a recorder of seawater isotopic signatures, *Quat. Sci. Rev.*, *88*, 1–13, doi:10.1016/j.quascirev.2013.12.027.

Tanaka, T. et al. (2000), JNdi-1: A neodymium isotopic reference in consistency with LaJolla neodymium, *Chem. Geol.*, *168*(3–4), 279–281, doi:10.1016/S0009-2541(00)00198-4.

Torsvik, T. H., S. Rousse, C. Labails, and M. A. Smethurst (2009), A new scheme for the opening of the South Atlantic Ocean and the dissection of an Aptian salt basin, *Geophys. J. Int.*, *177*(3), 1315–1333, doi:10.1111/j.1365-246X.2009.04137.x.

Tzedakis, P. C., M. Crucific, T. Mitsui, and E. W. Wolff (2017), A simple rule to determine which insolation cycles lead to interglacials, *Nature*, *542*(7642), 427–432, doi:10.1038/nature21364.

Vance, D., and K. Burton (1999), Neodymium isotopes in planktonic foraminifera: A record of the response of continental weathering and ocean circulation rates to climate change, *Earth Planet. Sci. Lett.*, *173*(4), 365–379, doi:10.1016/S0012-821X(99)00244-7.

Vance, D., A. E. Scrivner, P. Beney, M. Staubwasser, G. M. Henderson, and N. C. Slowey (2004), The use of foraminifera as a record of the past neodymium isotope composition of seawater, *Paleoceanography*, *19*(2), doi:10.1029/2003PA000957.

Wei, R., W. Abouchami, R. Zahn, and P. Masque (2016), Deep circulation changes in the South Atlantic since the Last Glacial Maximum from Nd isotope and multi-proxy records, *Earth Planet. Sci. Lett.*, doi:10.1016/j.epsl.2015.11.001.

Weijer, W., W. P. M. De Ruijter, and H. A. Dijkstra (2001), Stability of the Atlantic Overturning Circulation: Competition between Bering Strait freshwater flux and Agulhas heat and salt sources, *J. Phys. Oceanogr.*, *31*(8), 2385–2402, doi:10.1175/1520-0485(2001)031<2385:SOTAOC>2.0.CO;2.

Weijer, W., W. P. M. De Ruijter, A. Sterl, and S. S. Drijfhout (2002), Response of the Atlantic overturning circulation to South Atlantic sources of buoyancy, *Glob. Planet. Change*, *34*(3–4), 293–311, doi:10.1016/S0921-8181(02)00121-2.

APPENDICES

APPENDIX A: DATA FROM PREVIOUS STUDIES AND REPORTS

ND ISOTOPE DATA FROM THE SOUTHEAST ATLANTIC (HOWE ET AL., 2016)

Table 2. Data overview of sediment cores from the southeast Atlantic off the coast of southern Africa, which were analyzed for their (foraminiferal) ε_{Nd} ratios in previous studies. Holocene and LGM ε_{Nd} ratios and calculated %NADW for the study locations were derived from foraminiferal Nd isotopic composition. The references to the individual studies, as well as the ε_{Nd} measurement details are provided in the endnotes below the table (Howe et al. [2016c]).

				Holocene		**LGM**	
Core	**Latitude** (°N)	**Longitude** (°E)	**Depth** (mbsl)	ε_{Nd}	%NADW	ε_{Nd}	%NADW
GeoB 3603-2[1]	-35.1	17.6	2840	-10.1	40	-8.0	43
MD02-2594[1]	-34.7	17.3	2440	-9.7	32	-7.8	40
MD96 2085[2]	-30.0	13.0	3001	-10.6	50	-8.6	52
MD96 2086[2]	-25.8	12.1	3606	-11.8	73	-7.8	40
MD96 2098[2]	-25.6	12.6	2910	-12.2	81	-9.3	60
ODP 1088[2]	-41.0	13.5	2082	-8.4	0	-7.7	0
RC11 86[2]	-36.0	18.0	2829	-9.9	37	-8	43
RC13 228[2]	-22.0	11.0	3204	-11.7	72	-8.9	56
RC13 229[2]	-26.0	11.0	4191	-10.3	45	-7.7	39
RC13 253[2]	-46.0	7.0	2494	-8.5	0	-8.3	0
TNO57-21[3]	-41.1	7.9	4981	-9.1	17	-6.8	24
TTN057-6-PC4[2]	-42.9	8.6	3702	-9.4	23	-6.4	18

1: Wei et al. [2016]: Nd isotopic composition measured on mixed planktic foraminifera, Fe–Mn leachates and fish debris; ε_{Nd} presented here was measured on planktic foraminifera; %NADW calculated by Howe et al. [2016c]

2: Howe et al. [2016c]: Nd isotopic composition measured on mixed planktic foraminifera

3: Piotrowski et al. [2012]: Nd isotopic composition measured on mixed planktic foraminifera; %NADW calculated by Howe et al. [2016c]

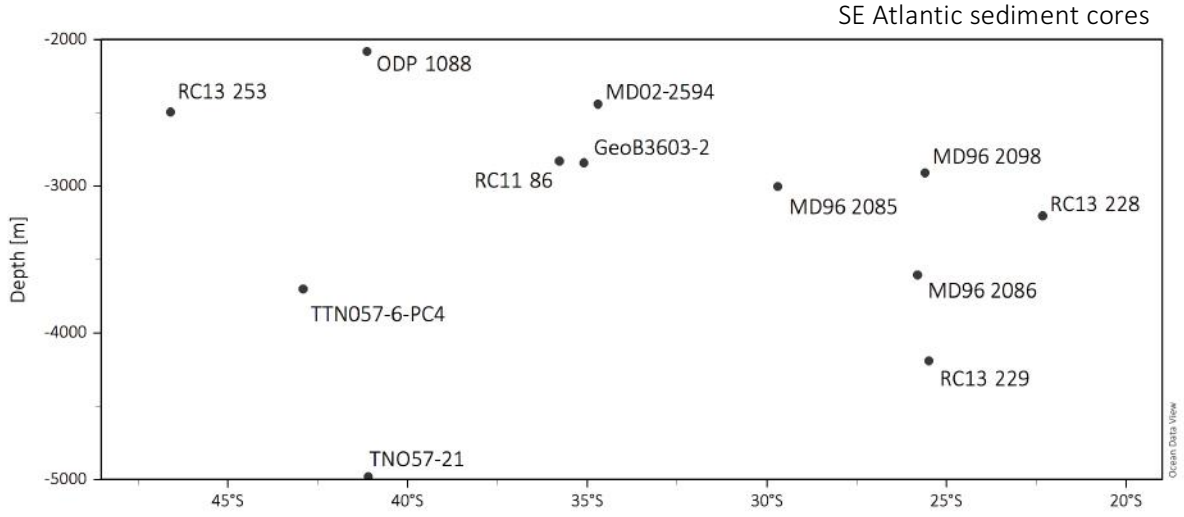

Figure 14. Cross-section indicating the location of the stations used to recreate the Holocene and LGM ε_{Nd} reconstruction

CORE DESCRIPTIONS AND L* PROFILES OF THE TOP METER OF GEOB8336-6 AND GEOB8342-6

As the samples were all taken from depth intervals in uppermost meter, the core description and L* profiles are only provided for the top 100 cm of the cores. The complete core descriptions and profiles can be found in the M57/3 cruise report [*Schneider et al.*, 2003] and the supporting material.

LEGEND

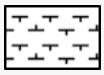

nanofossil bearing foraminifera ooze/
foraminifera bearing nanofossil ooze

SSS Strongly bioturbated

Figure 15. Legend explaining the lithographical pattern and structure symbols used for the sediment core description [derived from *Schneider et al.*, 2003]

GEOB8336-6

The first meter of GeoB8336-6 is dominated by strongly bioturbated foraminifera and cocolithophore ooze. The youngest sediment unit (0 to 23 cm) and the third unit (34 to 54 cm are very pale brown in color; the calcareous sediment ooze in between the two units is light yellowish brown (23 to 34 cm). Overall, the last unit is mostly light gray in color (54 to 204 cm), however, dark grayish brown "laminated" bands, possibly Mn precipitations, interrupt the unit on four occasions (86 to 90 cm, 119 to 120 cm, 126 to 129 cm, and 174 to 178 cm) [*Schneider et al.*, 2003].

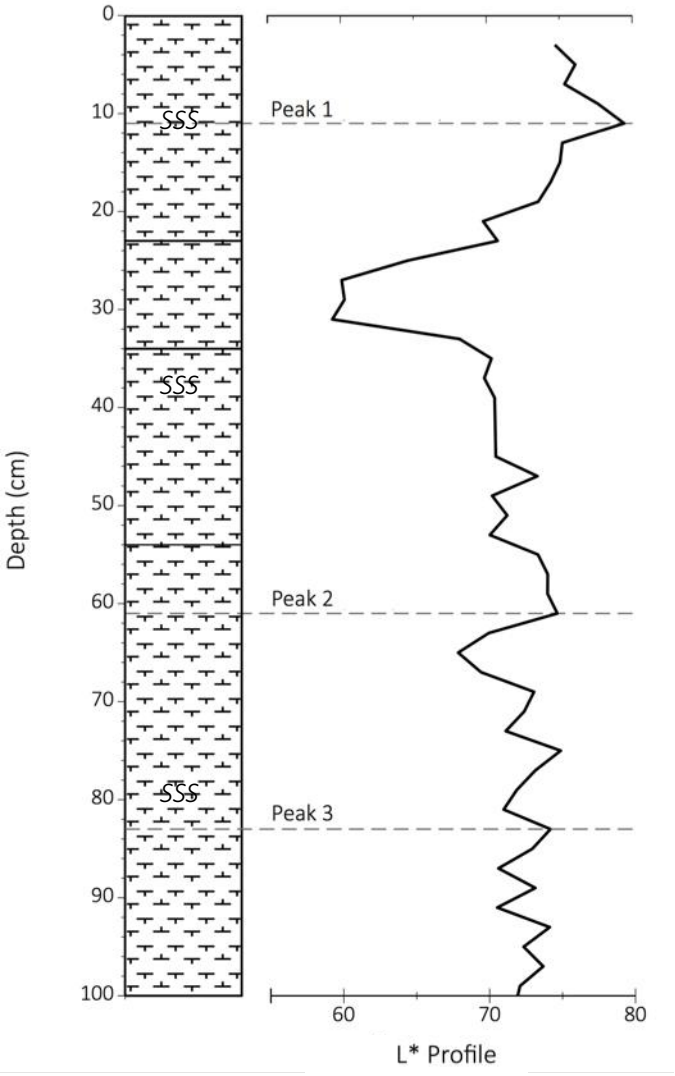

Figure 16. Sediment color reflectance (L*) profile of the first meter of GeoB8336-6 L* peak 1, peak 2 and peak 3 occurred at 11 cm, 61 cm and 83 cm, respectively. [figure taken and modified after *Schneider*, 2003a; via *Schneider et al.*, 2003].

GEOB8342-6

GeoB8342-6 is primarily composed of strongly bioturbated foraminifera and coccolithophore-bearing mud, which varies in color with depth. The first and youngest sediment unit (0 to 35 cm), and the third unit (53 to 78 cm) both appear pale yellow; the mud unit in between (35 to 53 cm) is light olive brown. The oldest unit of the upper meter (the fourth unit of the core; 78 – 278 cm) appears light greenish gray [*Schneider et al.*, 2003].

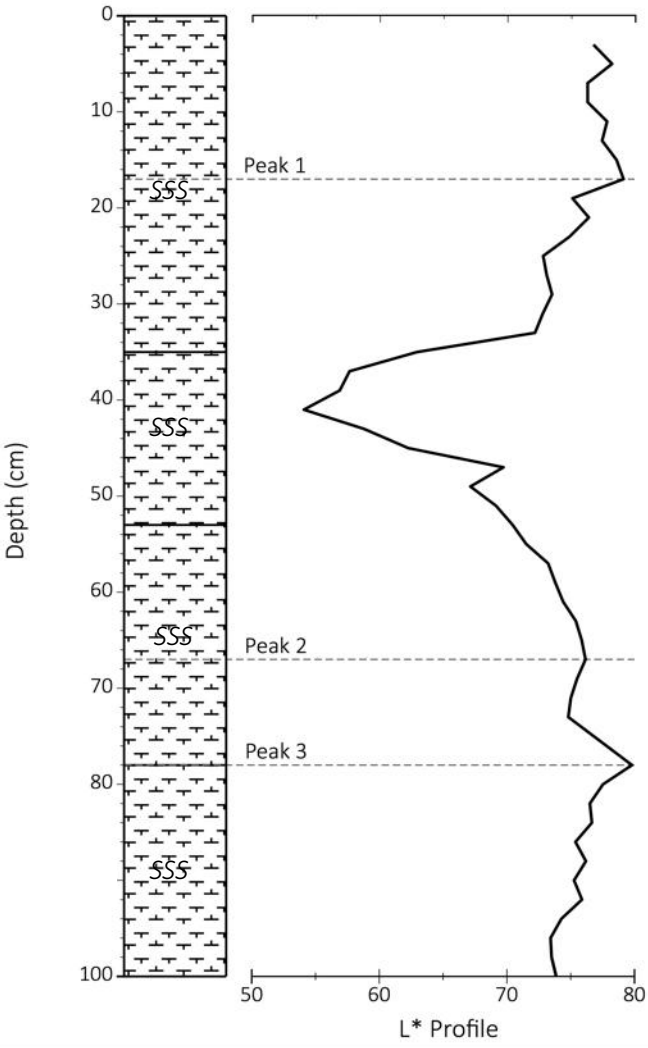

Figure 17. Down-core sediment color reflectance (L*) profile and simplified lithography of the first meter of GeoB8342-6

L* peak 1, 2 and 3 occur at 17 cm, 67 cm and 78 cm, respectively [figure taken and modified after *Schneider*, 2003b; via *Schneider et al.*, 2003].

APPENDIX B: PICTURES OF THE SAMPLES AND SAMPLE DESCRIPTIONS

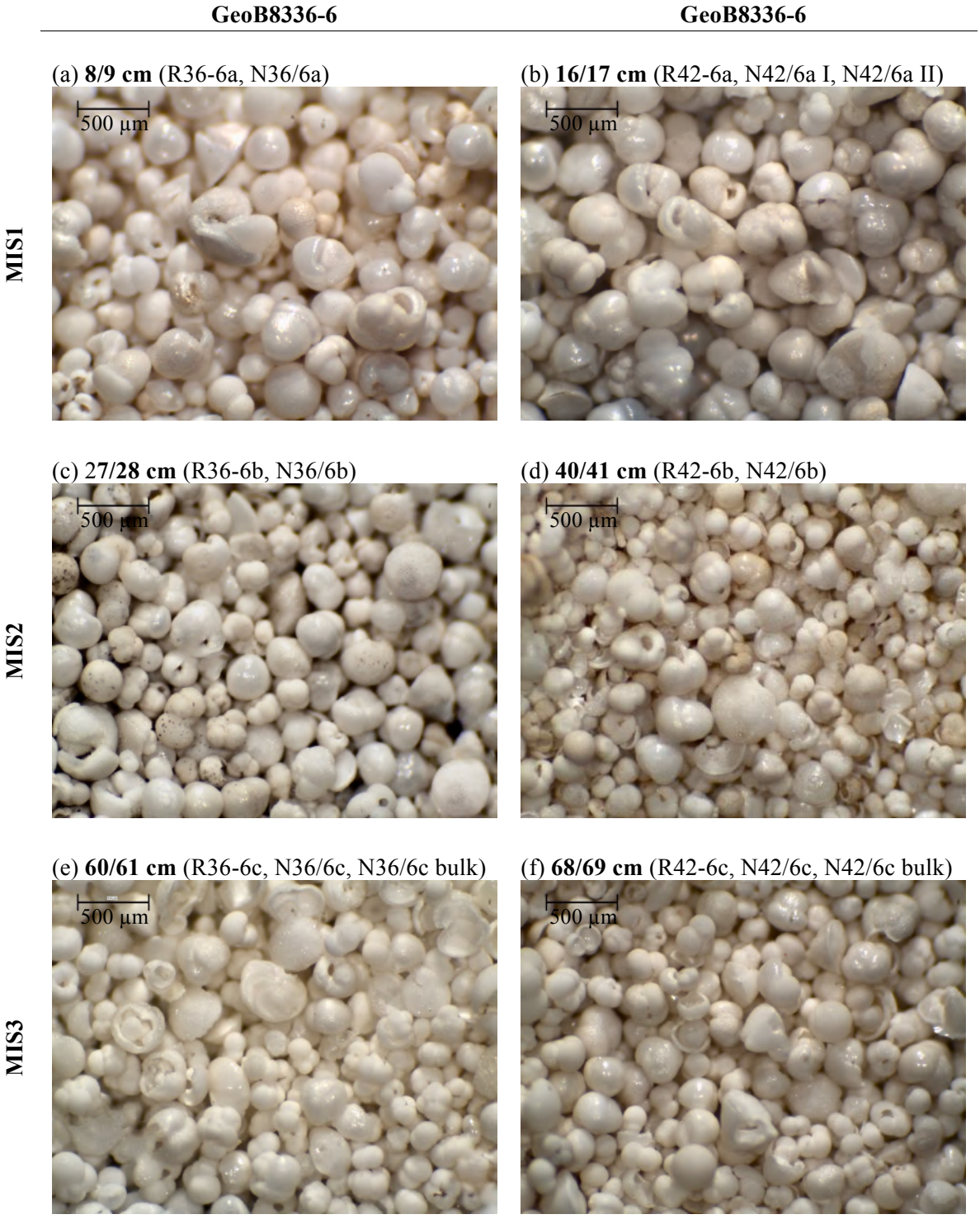

Figure 18 a-h. Pictures of the sand fraction (>63 µm) of the sample intervals considered in this study. The samples are almost entirely composed of planktic and benthic foraminifera (whole tests and fragments). Pictures obtained with the Leica EZ4 D microscope system at the University of Cape Town (Rebecca von Koslowski, March 2017)

Table 3. Sample description of the bulk samples (63 to 250 µm) analyzed for the REE pre-concentration measurements. "-a", "-b", and "-c" correspond to the MIS1, 2, and 3 depths in the core, respectively (5.1 Age model).

Sample	**Depth interval in core** (cm)	**Sample species**	**Weight** (mg)	**Sample description and remarks**
R36-6a	8/9	Mostly (whole) mixed planktic foraminifera	23	High abundance of *G. inflata;* some foraminifera tests had black, spotty coatings on them (possibly Mn oxides)
R36-6b	27/28	Mostly (whole) mixed planktic foraminifera	27	Most tests were showed some secondary coatings and were at least partially covered and/or filled with yellow/light brown crystalline coatings (likely Fe oxides/early diagenetic calcite that precipitated) or black (Mn) oxides
R36-6c	60/61	Mostly (whole) mixed planktic foraminifera	9	Some specimen were covered with yellow coatings, but significantly less than 36/6c
R42-6a	16/17	Mostly (whole) mixed planktic foraminifera	22	Some specimen were coated with yellow/light brown and black coatings
R42-6b	40/41	Mostly (whole) mixed planktic foraminifera	23	Most tests had at least some (Fe-oxide) coating; some tests were almost entirely covered in dark yellow/light brown coatings
R42-6c	68/69	Mostly (whole) mixed planktic foraminifera	12	Some tests contained oxide-coatings; glauconite grains were present in the sample and manually removed

Table 4. Sample description of the mixed planktic and bulk samples (>63µm) analyzed for their Nd isotope composition. "-a", "-b", and "-c" correspond to the MIS1, 2, and 3 depths in the core, respectively (5.1 Age model). The most important foraminifera species of the handpicked planktic samples are listed under 'notable species' – whenever one single species was very dominant, that species is denoted with '*'.

Sample	**Depth interval in core** (cm)	**Notable species**	**Weight** (mg)	**Test description & remarks**
N36-6a	8/9	*Globigerina bulloides* *G. inflata** *G. truncatulinoides*	30	Tests generally appear clean and most tests in the interval are whole. Few tests contain significant amounts of light yellow mud cemented to the walls of the tests' inner chambers
N36-6b	27/28	*Globigerinoides ruber (white)* *G. inflata* *Neogloboquadrina pachyderma (l)*	23	Most foraminifera have black coatings or yellow brown fillings; significantly lower abundance of whole tests than in N36-6a
N36-6c	60/61	*Globigerina bulloides* *G. inflata* *Neogloboquadrina pachyderma (l)** *O. universa*	25	No visible coatings on the exterior of the tests; some foraminifera have light yellow mud cemented to their inner chamber walls; *O. universa* generally appear light yellow
N36-6c bulk		*(bulk sample)*	29	High abundance of planktic species, especially *G. inflata*; many broken foraminifera shells; no black coatings present but some light yellow coatings on the inside
N42-6a I	16/17	*Globigerina bulloides* *G. inflata* *O. universa*	22	Tests show no discolorations on the outside; some reveal light yellow calcified mud fillings after being crushed
N42-6a II			21	
N42-6b	40/41	*Globigerina bulloides* *G. inflata* *Neogloboquadrina pachyderma (r)* *O. universa*	21	Strong yellow discoloration of most tests in this interval; black coatings are found on the outside of some tests but not as frequently as on those in N36/6b
N42-6c	68/69	*Globigerina bulloides* *G. inflata* *Neogloboquadrina pachyderma (r)* *O. universa*	20	Some tests had light yellow coatings and darker yellow fillings; very few have black coatings one the outside
N42-6c bulk		*(bulk sample)*	29	High abundance of planktic species; many broken tests; no single dominant species

APPENDIX C: REE PRE-CONCENTRATION MEASUREMENT DATA

Table 5. REE concentrations (in ppm) measured in the non-detrital fraction of bulk foraminifera samples from sediment cores GeoB8336-6 and GeoB8342-6. TPB denotes 'total procedural blank'. Concentrations are an average from three measurements. "%SD" denotes the standard deviation of the measurements given in %; concentrations of REE Pm were not measured.

	Bulk foraminifera sample												
Element	R36/6a	%SD	R36/6b	%SD	R36/6c	%SD	R42/6a	%SD	R42/6b	%SD	R42/6c	%SD	**TPB**
La	2.163	0.165	1.708	0.831	1.997	0.126	2.763	0.712	2.993	1.051	2.395	0.362	0.004
Ce	2.477	0.209	2.044	0.365	2.400	0.096	3.259	0.908	3.526	0.59	2.772	0.896	0.004
Pr	0.454	0.918	0.378	0.815	0.439	0.455	0.575	0.419	0.666	0.198	0.524	0.67	0.004
Nd	1.937	0.822	1.648	0.079	1.916	1.066	2.459	0.189	2.797	0.646	2.250	0.378	0.004
Sm	0.397	0.341	0.357	1.052	0.415	0.468	0.504	0.863	0.582	0.778	0.474	0.64	0.004
Eu	0.104	0.78	0.091	4.144	0.108	0.105	0.124	1.054	0.146	1.139	0.124	0.484	0.004
Gd	0.462	0.876	0.421	0.311	0.530	1.03	0.612	0.784	0.717	0.324	0.597	0.846	0.004
Tb	0.073	0.901	0.064	1.505	0.078	0.187	0.090	0.109	0.101	0.603	0.089	0.424	0.004
Dy	0.468	0.139	0.398	0.548	0.502	0.518	0.578	0.779	0.663	0.737	0.550	0.176	0.004
Ho	0.105	1.216	0.085	0.56	0.104	0.106	0.122	0.907	0.137	0.534	0.113	0.873	0.004
Er	0.308	0.112	0.237	0.131	0.298	0.578	0.373	0.117	0.398	0.924	0.322	0.366	0.004
Tm	0.046	1.542	0.033	0.984	0.042	1.117	0.050	1.61	0.053	0.358	0.046	1.532	0.004
Yb	0.270	0.792	0.204	0.441	0.269	0.241	0.327	0.594	0.349	0.496	0.276	0.902	0.004
Lu	0.047	0.48	0.033	0.283	0.041	1.376	0.051	1.64	0.054	0.827	0.044	1.185	0.004

Table 6. PAAS-normalized REE concentrations of bulk foraminifera samples from sediment cores GeoB8336-6 and GeoB8342-6.

Element	**Bulk foraminifera sample**					
	R36/6a	**R36/6b**	**R36/6c**	**R42/6a**	**R42/6b**	**R42/6c**
La	0.0566	0.0447	0.0523	0.0723	0.0784	0.0627
Ce	0.0311	0.0257	0.0306	0.0409	0.0443	0.0348
Pr	0.0514	0.0428	0.0497	0.0651	0.0754	0.0593
Nd	0.0571	0.0486	0.0565	0.0725	0.0825	0.0664
Sm	0.0715	0.0643	0.0748	0.0908	0.105	0.0854
Eu	0.0963	0.0843	0.100	0.115	0.135	0.1148
Gd	0.0991	0.0903	0.114	0.131	0.154	0.1281
Tb	0.0943	0.0827	0.101	0.116	0.130	0.115
Dy	0.100	0.0850	0.107	0.124	0.142	0.1175
Ho	0.106	0.0858	0.105	0.123	0.138	0.114
Er	0.108	0.0832	0.105	0.131	0.140	0.113
Tm	0.114	0.0815	0.104	0.123	0.131	0.114
Yb	0.0957	0.0723	0.0954	0.116	0.124	0.0979
Lu	0.108	0.0762	0.0947	0.118	0.125	0.102

Table 7. Ratios and calculated anomalies of bulk foraminifera samples from sediment cores GeoB8336-6 and GeoB8342-6. Equations were taken from Bolhar et al. [2004] (1), Bau and Dulski [1996] (2), and Martin et al. [2010] (3)

	Bulk foraminifera sample							
	R36/6a	**R36/6b**	**R36/6c**	**R42/6a**	**R42/6b**	**R42/6c**	**Equation**	**References**
$(Pr/Yb)_{SN}$	0.54	0.59	0.52	0.56	0.61	0.61	-	(1)
$(Ce/Ce^*)_{SN}$ (A)*	0.68	0.69	0.70	0.71	0.65	0.67	1	(1)
$(Ce/Ce^*)_{SN}$ (B)$^+$	0.58	0.59	0.59	0.60	0.58	0.57	2	(2)
$(Pr/Pr^*)_{SN}$§	1.17	1.15	1.15	1.15	1.19	1.17	3	(2)
$(Eu/Eu^*)_{SN}$	1.22	1.20	1.20	1.16	1.19	1.21	4	(2)
$(Gd/Gd^*)_{SN}$	1.12	1.12	1.21	1.20	1.29	1.14	5	(2)
$[MREE/MREE^*]_{SN}$	1.22	1.41	1.42	1.31	1.38	1.45	6	(3)

1 : $(Ce/Ce^* * A)_{SN} = [Ce_{SN}/(2 * Pr_{SN} - Nd_{SN})]$

2 : $(Ce/Ce^* * B)_{SN} = [Ce_{SN}/(0.5 * La_{SN} + 0.5 * Pr_{SN})]$

3 : $(Pr/Pr^*)_{SN} = [Pr/(0.5 * Ce_{SN} + 0.5 * Nd_{SN})]$

4 : $(Eu/Eu^*)_{SN} = [Eu/(0.67 * Sm_{SN} + 0.33 * Tb_{SN})]$

5 : $(Gd/Gd^*)_{SN} = [Gd_{SN}/(0.67 * Tb_{SN} + 0.33 * Dy_{SN})]$

6 : $([MREE]/[MREE^*])_{SN} = [2 * (Gd + Tb + Dy)_{SN}/(La + Pr + Nd + Tm + Yb + Lu)_{SN}]$

APPENDIX D: ND ISOTOPE MEASUREMENT DATA

Table 8. Neodymium isotope measurements (with 2σ errors) from the Multicollector ICP-MS analysis and calculated neodymium isotope systematics of foraminifera samples from GeoB8336-6 and GeoB8342-6, the UCT internal carbonate standard NM95, and the reference values of the standard of JNdi-1 used to correct the samples [*Tanaka et al.*, 2000]. NM95 had not been previously analyzed for its Nd isotope composition so no reference data were available. ε_{Nd} ratios were calculated using the equation presented in I Introduction [*Jacobsen and Wasserburg*, 1980].

	Measured and calculated Nd systematics				
Sample	**$^{143}Nd/^{144}Nd$**	**2σ**	**ε_{Nd}**	**2σ**	**Remarks**
N36/6a	0.512087	±0.000017	-10.7	±0.3	
N36/6b	0.512224	±0.000015	-8.1	±0.3	
N36/6c	0.512188	±0.000013	-8.8	±0.3	mean ε_{Nd} ~ -8.75±0.30
N36/6c bulk	0.512193	±0.000016	-8.7	±0.3	
N42/6a I	0.512124	±0.000019	-10.0	±0.4	mean ε_{Nd} ~ -10.20±0.40
N42/6b II	0.512107	±0.000019	-10.4	±0.4	
N42/6b	0.512241	±0.000014	-7.7	±0.3	
N42/6c	0.512196	±0.000018	-8.6	±0.4	mean ε_{Nd} ~ -8.70±0.35
N42/6c bulk	0.512185	±0.000014	-8.8	±0.3	
NM95	0.512101	±0.000020	-	-	
Ref. JNdi-1	0.512115	±0.000007	-	-	